Economic Geology
Vol. 96, 2001, pp. 271–305

Geologic Evolution of the Escondida Area, Northern Chile: A Model for Spatial and Temporal Localization of Porphyry Cu Mineralization

Jeremy P. Richards,†

Department of Earth and Atmospheric Sciences, University of Alberta, Edmonton, Alberta, Canada T6G 2E3

Adrian J. Boyce, and Malcolm S. Pringle

Scottish Universities Research and Reactor Centre, Scottish Enterprise Technology Park, Rankine Avenue, East Kilbride G75 0QF, Scotland, United Kingdom

Abstract

A program of geologic mapping and lithogeochemical and geochronological sampling has been carried out over a 745-km^2 area of the Atacama Desert surrounding the porphyry Cu deposits at Escondida, Zaldívar, and Chimborazo (Cordillera de Domeyko, northern Chile). The purpose of this study was to examine the regional tectonic and magmatic setting of this preeminent porphyry Cu district for evidence of features or processes that might explain the giant scale of mineralization at Escondida and provide predictive tools for exploration in other areas.

The geologic history of this area as recorded by exposed rocks begins with voluminous, intermediate to felsic Permo-Carboniferous volcanism (La Tabla Formation), and these rocks appear to constitute the crystalline basement throughout much of the porphyry belt of northern Chile. Geochemically, they are I-type in character, but the parental magmas were relatively dry, and thus did not generate effective magmatic-hydrothermal systems (few significant ore deposits are known to be associated with them).

Andean cycle arc magmatism began in the Triassic, centered on the La Negra magmatic arc (now located near the Chilean coast). Farther inland, near Escondida, back-arc processes led to the eruption of intermediate to felsic lavas and tuffs and the deposition of marine sediments in rift basins. Closure of these basins in the Late Cretaceous resulted in deformation of the volcano-sedimentary sequences and was followed by emplacement of small alkali gabbro stocks and dikes.

The axis of arc magmatism moved eastward in the Paleocene (Central Valley arc) and produced widespread calc-alkaline intermediate to felsic volcanism through to the Eocene. East- to northeast-directed convergence maintained a dextral transpressive regime during this period, and early movements in the West Fissure zone, a corridor of orogen-parallel faults that runs the length of the Cordillera de Domeyko (over 1,000 km), reflect this couple. At the end of the Eocene, however, stresses in the arc appear to have relaxed, and by the late Oligocene, strike-slip movement along the West Fissure zone had reversed to sinistral. This period of stress relaxation at the end of the Eocene period coincided with the voluminous emplacement of dioritic magmas at shallow crustal levels and also with porphyry development.

Six samples of hornblende from these diorites yield $^{40}Ar/^{39}Ar$ dates between 38.28 ± 0.32 and 36.94 ± 0.46 Ma (2σ). Porphyry emplacement at Escondida, Zaldívar, and Chimborazo was coeval with this dioritic magmatism at ~38 Ma. Where plutonism was intense, the dioritic magma is interpreted to have evolved by processes of assimilation and fractional crystallization to more felsic compositions characteristic of the ore-forming porphyry intrusions. Whole-rock trace element data indicate that hornblende fractionation was an important control on chemical evolution of the diorites and attests to high-magmatic water contents (≥4 wt % H_2O). Volatile saturation would have occurred during further differentiation of these magmas, evidence for which is provided by the porphyry ore deposits.

Porphyry emplacement was localized within a broad zone of intersection between the West Fissure zone and a regionally extensive northwest-trending structural corridor (the Archibarca lineament). It is proposed that the geometry of this junction was conducive to the formation of transtensional pull-apart structures during relaxation or reversal of dextral shear on the West Fissure zone. Such dilational structures would have focused the ascent and pooling of magma in the upper crust and maximized the potential for formation of magmatic-hydrothermal ore deposits.

The formation of giant porphyry systems such as Escondida is, therefore, considered to be the result of a fortuitous coincidence of processes, including generation of suitable volumes and compositions of magma, appropriate lithospheric stress conditions, and structural focusing of emplacement; in addition, the development of thick supergene enrichment blankets has been critical to the economic value of these deposits. None of these contributory processes are in themselves unusual or rare, but because they are largely independent of one another, their constructive cooperation in ore formation is not necessarily repeatable at different places and at different times, thus explaining the relative rarity of giant porphyry deposits.

Introduction

Northern Chile is the world's premier porphyry copper district, hosting several major deposits such as Collahuasi, Chuquicamata, Spence, Escondida, and El Salvador, as well as many smaller and subeconomic deposits. The majority of the largest deposits, including those named above, lie in a narrow, 30- to 50-km-wide, orogen-parallel belt that stretches over 1,000 km from 28° S to 19° S and perhaps beyond into

† Corresponding author: e-mail, Jeremy.Richards@UAlberta.CA

southern Peru at 18° S (Clark et al., 1998). This belt is known as the West Fissure zone) and is named after a prominent north-south strike-slip fault (the West Fissure, or Falla Oeste) that offsets ore in the Chuquicamata deposit (López, 1939; Fig. 1). It is also referred to as the Sistema de Falla de Domeyko, after the Cordillera de Domeyko to which it forms the western boundary with the Depresión Intermedia (Central Valley).

The West Fissure zone is characterized by a corridor of orogen-parallel faults with a history of strike-slip and normal movement dating back at least to the late Eocene (Maksaev and Zentilli, 1988) and perhaps finding its origin in late Paleozoic and Mesozoic rift faults (Günther et al., 1997). During the late Eocene and early Oligocene, the line of the West Fissure zone coincided with the eastern margin of the Andean magmatic arc, and calc-alkalic volcanism and plutonism were focused along its length. Porphyry Cu-generating intrusions were emplaced along the West Fissure zone at a late stage in this magmatic cycle, typically constituting the last significant plutonic phase in any given area (e.g., Maksaev and Zentilli, 1988; McKee and Noble, 1989; Hammerschmidt et al., 1992).

Although the first-order structural control on localization of porphyry systems exercised by the West Fissure zone has been known for many years, a second-order control has been recognized more recently in the form of northeast- and northwest-trending cross-orogen lineaments, which appear to mark the loci of some of the largest porphyry centers where they intersect the West Fissure zone (Fig. 1; Salfity, 1985; Salfity and Gorustovich, 1998; Abels and Bischoff, 1999). The nature and origin of these lineaments is not clear, however; nor is the mechanism by which they appear to have focused igneous intrusive activity.

In order to begin to address these questions, a detailed study of the regional geology around one such intersection, between the Archibarca lineament and the West Fissure zone, has been conducted. Located within this intersection zone is the world's largest (in terms of production) porphyry Cu mine, Escondida, as well as the Zaldívar mine and the Chimborazo deposit.

In this paper, the results of regional mapping over an area of approximately 745 km^2 around the Escondida-Zaldívar-Chimborazo systems are reported (Figs. 2 and 3), supplemented by $^{40}Ar/^{39}Ar$ dating (see also Richards et al., 1999), and whole-rock geochemical data for key lithologies. The metalliferous porphyry systems are shown to be coeval with a period of voluminous dioritic plutonism in the late Eocene and to be located to within 10 km of the intersection of the West Fissure zone and the northwest-trending Archibarca lineament.

Mapping program

Fieldwork was carried out by the first author over four field seasons (4 to 6 weeks each) between 1993 and 1998, using field vehicles, support personnel, and camping equipment provided by RTZ Mining and Exploration Ltd. (1993–1995) and Minera Outokumpu Chile S.A. (1998). Mapping was conducted at a scale of 1:50,000, using topographic maps based on the UTM grid (Figs. 2 and 3); hand-held global positioning system units were used for navigation, providing coordinates of locations to better than ±30 m.

The Atacama Desert is an ancient landscape, and much of the area is covered by Oligo-Miocene alluvial fan gravels and younger salars, rendering bedrock mapping difficult. Rising out of the gravel floor of the desert are isolated hills and ridges of more resistant rock types, the margins of which are frequently fault or lithologically controlled, as are other topographic features such as dry river valleys (quebradas) and scarps. The flanks of these topographic highs are draped with talus, and it is rarely possible precisely to locate geologic contacts or structures. In addition, true outcrop is rare, typically being restricted to the peaks of hills and to quebradas (which are periodically deepened by flash floods). Extrapolation of geology beneath the gravel cover is tentative, therefore, and structures extended through these areas as shown in Figure 3 are interpretations.

Geologic Evolution of the Central Andes

The western margin of South America has been a destructive plate boundary since the Mesozoic, when it formed the western seaboard of Gondwana. Prior to this time, basement rocks record a series of apparently ensialic events during the Late Proterozoic and Paleozoic eras, characterized by the emplacement of predominantly S-type granitoids, eruption of coeval volcanic materials, and periodic metamorphism. The geologic framework of the central Andes of northern Chile and northwestern Argentina is reviewed below and summarized with references in Table 1.

Late Proterozoic and Paleozoic

The Precambrian and early Paleozoic history of the central Andes is not well known, with evidence available only from scattered, disconnected basement outcrops. Nevertheless, a picture emerges of activity within a mainly cratonic setting related to development of ensialic rifts and basins and periods of compression possibly associated with terrane accretion events. Four main cycles of tectonism are recognized in this region by Damm et al. (1990, 1994), the first three of which (Pampean, Panamerican, and Caledonian cycles; Table 1) are known only through correlations of sparse basement age data with established events elsewhere.

The latest pre-Mesozoic event, relating to the Hercynian (Variscan) orogeny, is much better represented in basement rocks of the central Andes. Intrusive and extrusive S-type igneous rocks with associated periods of metamorphism were generated throughout the Carboniferous (from ~350 Ma) and Permian (to ~240 Ma; Damm et al., 1994). Extensive areas of Hercynian granites and felsic to intermediate volcanic and subvolcanic rocks (La Tabla Formation of the field area) are exposed as uplifted blocks throughout the central Andes and include the Cordillera de Domeyko within the present study area, the Sierras de Varas and Argomedo (to the immediate south), and the Sierra de Limón Verde to the north (see references in Table 1). The frequency of inherited late Paleozoic zircons found in younger Tertiary granitoids from throughout this region suggests that Hercynian materials constitute a large part of the pre-Andean basement (Zentilli et al., 1994; Cornejo et al., 1997; Richards et al., 1999).

Mesozoic and Cenozoic: Andean cycle

The start of the Andean cycle was a diachronous event relating to the breakup of the Gondwana supercontinent. In the

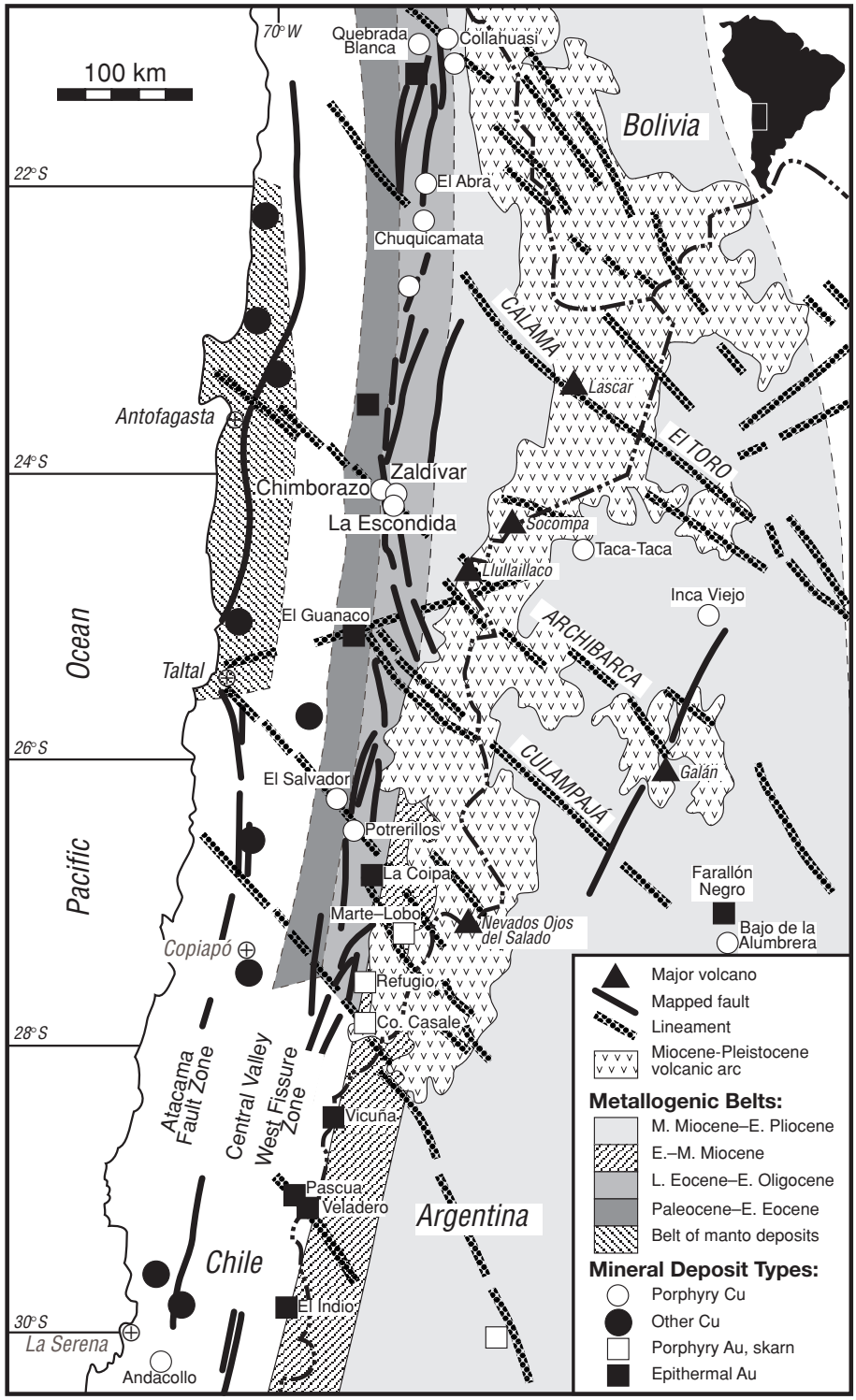

FIG. 1. Regional geologic sketch map of northern Chile, showing the locations of major Cu and Au deposits in relationship to arc-parallel belts of coeval magmatism (after Sillitoe, 1992), and regional-scale faults and lineaments (modified from Salfity, 1985; Salfity and Gorustovich, 1998). The largest porphyry Cu deposits are located within the West Fissure zone and clusters of deposits occur in the vicinity of intersections between the zone and northwest-trending cross-orogen lineaments identified by Salfity (1985) and Salfity and Gorustovich (1998). One such intersection occurs in the Escondida district, where the Archibarca lineament crosses the West Fissure zone. Note that Salfity (1985) and Salfity and Gorustovich (1998) include known faults, stratigraphic discontinuities and changes, volcanic lineations, and topographic features identified from air and satellite images in their interpretation of lineaments (cf. Heyl, 1972). In many cases, the exact geologic nature of these lineaments and their intersections is unclear, and an objective of this paper is to document in detail one such intersection in the Escondida area.

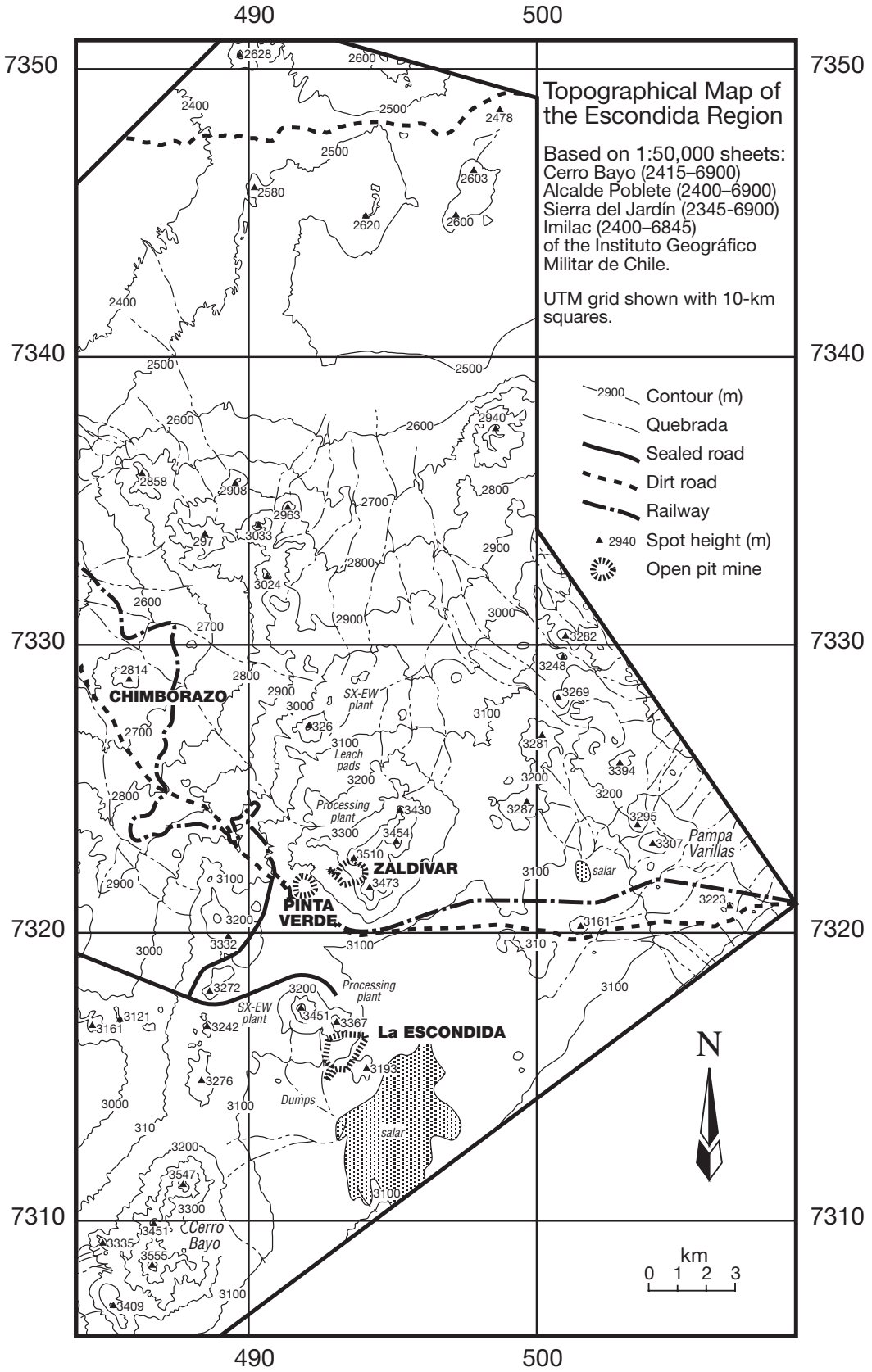

FIG. 2. Topographic map of the study area, showing the locations of the Escondida, Zaldívar, and Pinta Verde open-pit porphyry Cu mines, and the Chimborazo prospect. Redrawn and modified from 1:50,000 topographical sheets published by the Instituto Geográfico Militar de Chile.

This is the page the fold-out map is on

Back of fold-out map

TABLE 1. Tectonic Framework of the Chilean Central Andes

Period	Age range (Ma)	Tectonic event	Tectonic and magmatic behavior	Manifestation in Escondida region	References
Late Miocene-early Pliocene		Flattening of subduction angle; continued eastward migration of arc to Cordillera Occidental	Silicic volcanism; local ignimbrite eruption in Cordillera de Domeyko	Minor tuff horizons intercalated with gravels	Coira et al. (1982) Lahsen (1982) Kay et al. (1987) Maksaev and Zentilli (1988) de Silva (1989)
Middle Miocene-present	~15–0	Desertification		Desert conditions; cessation of erosion and preservation of supergene Cu enrichment blankets	Mortimer (1973, 1980) Maksaev and Zentilli (1988)
Late Oligocene-middle Miocene		Quechua tectonic phase: Onset of spreading on East Pacific Rise with renewed rapid east-northeast–directed convergence and flattening of subduction angle	Migration of magmatic arc to east (Cordillera Occidental); folding, arc-parallel sinistral strike-slip faulting, and high-angle reverse faulting in Cordillera de Domeyko	Uplift, erosion (Atacama gravels), and supergene Cu enrichment of porphyry deposits; sinistral fault movements in the WFZ	Mortimer (1973) Coira et al. (1982) Pardo-Casas and Molnar (1987) Alpers and Brimhall (1988) Maksaev and Zentilli (1988) Mpodozis and Ramos (1989) Scheuber et al. (1994) Sillitoe and McKee (1996) Tomlinson and Blanco (1997b)
Late Eocene-early Oligocene	38–35	End of Incaic tectonic phase	Relaxation of transpressive stress in the Cordillera de Domeyko	Emplacement of diorite plutons and porphyry Cu systems in transtensional structures within the WFZ	Richards et al. (1999) This paper
Late Eocene-early Oligocene(?)	~38.5	Incaic tectonic phase: Slower, oblique (northeast-directed) convergence	Arc-normal shortening, folding, arc-parallel dextral transpressive faulting; cessation of volcanic activity in Precordillera	Uplift, dextral fault movements in the WFZ	Frutos (1981, 1988) Maksaev and Zentilli (1988) Mpodozis and Ramos (1989) Hammerschmidt et al. (1992) Scheuber and Reutter (1992) Scheuber et al. (1994) Lindsay et al. (1995) Reutter et al. (1996) Tomlinson and Blanco (1997a)
Middle-late Eocene	47.8–38.5	Continued rapid convergence; migration of arc to east	Precordillera magmatic arc develops	Continued calc-alkalic volcanism (Augusta Victoria Fm.) and dioritic plutonism	Coira et al. (1982) Pilger (1983) Dalziel (1986) Pardo-Casas and Molnar (1987) Padilla (1988) Mpodozis and Ramos (1989) Hammerschmidt et al. (1992)
Paleocene-early Eocene	59–52	Rapid convergence	Central Valley magmatic arc develops; sparse development of porphyry Cu deposits (e.g., Cerro Colorado)	Calc-alkalic volcanism (Augusta Victoria Fm.)	Sillitoe (1992)
Late Cretaceous		Increased sea-floor spreading rate	Renewed arc magmatism	Emplacement of scattered gabbroic intrusions	Coira et al. (1982) Dalziel (1986) Padilla (1988)
Early-Late Cretaceous	130–80	Atlantic opening	Arc-normal shortening and closure of back-arc basin: Northwest-striking folds and thrusts	Uplift and deformation of Mesozoic volcano-sedimentary sequences	Dalziel (1986) Palacios et al. (1993)
Triassic-Early Cretaceous		Start of Andean cycle	La Negra magmatic arc and ensialic Tarapacá back-arc basin related to Gondwana breakup	Felsic to intermediate volcanism (Agua Dulce Fm.); siliciclastic and carbonate sedimentation (El Profeta, Santa Ana Fms.)	Coira et al. (1982) Mpodozis and Cornejo (1997) Mpodozis and Ramos (1989) Ardill et al. (1998)

TABLE 1. (*Cont.*)

Period	Age range (Ma)	Tectonic event	Tectonic and magmatic behavior	Manifestation in Escondida region	References
Carboniferous-Permian	350–240	Hercynian (Variscan) cycle	Arc magmatism	Granitic-granodioritic plutonism; coeval felsic to intermediate lavas, ignimbrites, and calderas (La Tabla Fm.)	Bahlburg and Hervé (1997) Coira et al. (1982) Davidson et al. (1985) Padilla (1988) Mpodozis and Ramos (1989) Damm et al. (1990, 1994) Andriessen and Reutter (1994) Smoje and Marinovic (1994) Franz and Lucassen (1997)
Ordovician-Silurian		Caledonian cycle (Oclóyic orogeny)	Terrane accretion		Mpodozis and Ramos (1989) Damm et al. (1990) Bahlburg and Hervé (1997)
Late Proterozoic-Cambrian		Panamerican cycle	Terrane accretion?		Mpodozis and Ramos (1989) Damm et al. (1990)
Middle Proterozoic	1460–1210	Pampean cycle	Development of ensialic margin		Coira et al. (1982) Damm et al. (1994)

Notes: In addition to the specific references listed in the Table, regional geological overviews are given by Jordan and Gardeweg (1989), Boric et al. (1990), and Frutos (1990). Abbreviations: Fm. = Formation; QFP = quartz-feldspar porphyry; WFZ = West fissure zone

central Andes, a magmatic arc and ensialic back-arc basin were developed in the Triassic to Early Cretaceous periods, with eruption of andesitic lavas and felsic tuffs (Triassic: Agua Dulce Formation) and deposition of thick sequences of carbonate and siliciclastic sediments (Triassic–Jurassic: El Profeta and Santa Ana Formations) in the study area. Opening of the Atlantic Ocean began at ~127 Ma, resulting initially in cessation of back-arc activity, uplift of the Paleozoic basement to form the proto-Cordillera de Domeyko, and deformation of these Mesozoic volcano-sedimentary sequences (Dalziel, 1986).

Subsequent changes in the pole of rotation of South America with respect to Africa, combined with a global increase in sea-floor spreading rates, resulted in a resumption of arc magmatism in the Late Cretaceous, which continues to the present day (Coira et al., 1982; Dalziel, 1986). This magmatic arc has migrated steadily eastward relative to the plate boundary, with periods of intense activity marked by orogen-parallel belts of coeval intrusive and volcanic rocks.

The arc passed through the Precordillera during the Eocene, marked by extensive andesitic to rhyolitic volcanism (Augusta Victoria Formation). This prominent magmatic event appears to correlate with a period of rapid, oblique (northeast-directed) convergence between the Nazca and South American plates, with subduction at a fairly steep and constant angle (Pilger, 1983; Pardo-Casas and Molnar, 1987). Slowing of the convergence rate toward the end of the Eocene was marked by a period of strong tectonism (Incaic phase), resulting in northwest-oriented folding and dextral strike-slip movements along the West Fissure zone and a cessation of volcanism (Scheuber and Reutter, 1992). The stress field within the arc appears to have reversed at the end of this tectonic phase, and it is argued below that transtensional movements within the West Fissure zone at this time facilitated emplacement of late Eocene-early Oligocene diorites and felsic porphyry systems. These intrusions typically represent the last mid-Tertiary igneous activity in the Precordillera, the arc then moving farther eastward in response to a renewed increase in convergence rate and flattening of the subduction angle.

The late Oligocene Quechua phase saw the development of the classic Andean margin, characterized by rapid (≥10 cm/yr), high-angle convergence, and uplift of the Andean mountain belt (Coira et al., 1982; Pardo-Casas and Molnar, 1987). In the Precordillera, this event was marked by pediplain formation and deposition of the Atacama gravels. It was also a period of critical importance for the development of ore in the porphyry Cu deposits, because uplift and erosion exposed these systems to supergene enrichment processes. In a second stroke of good fortune, a change in Pacific Ocean currents (development of the cool Humboldt current) and related weather conditions along the western seaboard of northern Chile in the middle Miocene (~15 Ma) caused the onset of desertification (Alpers and Brimhall, 1988). Erosional and weathering processes were therefore halted before they could destroy the transient Cu enrichment blankets that they had generated. Apart from local ignimbritic conflagrations and deep canyon formation resulting from occasional flash floods, the Precordillera has remained almost unchanged since this time, with millions of years of wind erosion sculpting a remarkable and beautiful stony desert.

Structural evolution

The Andean tectonic cycle is characterized by transpressional and transtensional movements along arc-parallel fault zones, with minor, but nonetheless important, strike-slip movements on northeast- and northwest-trending cross-orogen structures. Establishing a detailed chronology of movements on these structures has proved difficult, not least because slip directions seem to have reversed on several occasions.

Throughout most of the Cenozoic, subduction directions have been either normal (east directed) or oblique (northeast directed) to the Chilean coastline, such that the principal stress direction would be expected to produce compression and shortening, or arc-parallel dextral strike-slip movements, respectively, in the upper continental plate. Although such deformation did indeed occur, there is also evidence for periods of extension, transtension, and sinistral motion on arc-parallel structures in this region throughout the Mesozoic and Tertiary periods (e.g., Scheuber and Reutter, 1992; Brown et al., 1993; Flint et al., 1993; Mpodozis and Allmendinger, 1993; Scheuber et al., 1994; Reutter et al., 1996; Tomlinson and Blanco, 1997b). Thus, despite the Andes commonly being held to represent the classic compressional destructive margin, for significant periods throughout its history regions of both the back- and fore-arc have been under tension or transtension, with important implications for magma genesis and emplacement (cf. Hamilton, 1981; Weaver et al., 1987). For example, the intrusion of shallow-level granitic plutons is thought to be aided by transtensional structures such as pull-apart basins (rhombochasms or dilational jogs; Bussell, 1976; Hutton, 1988; Glazner, 1991; Petford and Atherton, 1992; Pitcher, 1997), whereas deep crustal batholith formation and effusive volcanism may dominate during periods of general compression (Glazner, 1991; Grocott et al., 1994; Takada, 1994; McNulty et al., 1998). A comprehensive knowledge of the history of deformation in the orogen would be useful, therefore, in understanding the observed cycles of volcanicity and plutonism and, in particular, their relationships to porphyry magmatism.

A review of the literature reveals many seemingly contradictory interpretations of fault movement directions on the two main arc-parallel systems, the West Fissure zone and the Atacama fault zone. The Atacama fault zone marks the position of the older Mesozoic (La Negra) arc and appears to have experienced sinistral or transtensional movement throughout this period (Reutter and Scheuber, 1988; Scheuber and Andriessen, 1990; Brown et al., 1993; Palacios et al., 1993). According to Scheuber and Andriessen (1990), sinistral shear is consistent with Mesozoic plate reconstructions that show southeast-directed subduction beneath the north Chilean margin. However, recent fault motions also appear to be sinistral, and such displacements are harder to reconcile with current east-northeast–directed convergence (Armijo and Thiele, 1990).

At the end of the Mesozoic period, an increase in sea-floor spreading rate and the opening of the Atlantic resulted in a change to northeasterly convergence along the Chilean margin and movement of the volcanic arc inland (Table 1). The Atacama fault zone, now being located in the fore arc, was under compression for much of the Tertiary, and strike-slip movement in the upper plate was transferred to the West Fissure zone by the late Eocene, marking the eastern edge of the Precordillera (Central Valley) arc. Dextral displacements in the West Fissure zone are documented in the late Eocene and possibly into the early Oligocene, although offsets probably did not exceed ~2 km (Maksaev and Zentilli, 1988; Reutter et al., 1991, 1996; Palacios et al., 1993; Lindsay et al., 1995; see also Yáñez et al., 1994, and Tomlinson and Blanco, 1997a, who suggest a period of sinistral movement in the mid-late Eocene). Eocene transpressive tectonism reflects strong coupling between the upper and lower plates in the subduction zone. The Central Valley arc was the focus of widespread volcanicity at this time, consistent with the theory noted above that volcanism is favored over shallow plutonism during periods of arc compression. By the end of the early Oligocene (after ~31 Ma), however, strike-slip motion in the West Fissure zone had reversed, and a well-documented period of sinistral displacement, resulting in a net offset of approximately 37 km in the Chuquicamata-El Abra area, ensued up to the middle Miocene (~17 Ma; Baker and Guilbert, 1987; Reutter et al., 1996; Dilles et al., 1997; Tomlinson and Blanco, 1997b). The exact timing of this reversal is not well constrained and may have been diachronous or intermittent along the length of the West Fissure zone from the late Eocene to the early Oligocene. Given that the convergence direction did not change during this period, the switch from dextral to sinistral orogen-parallel displacement presumably reflects a reversal of horizontal stress orientation in the upper plate. One possible explanation for this reversal is that reduction of coupling between the upper and lower plates resulted in a change from northeast-directed transpression to southwest-directed transtension in the Precordillera (Reutter et al., 1996).

Of great significance from the point of view of metallogeny is that this transition period from dextral to sinistral shear coincides broadly with the timing of late Eocene-early Oligocene porphyry Cu formation in the West Fissure zone and the cessation of volcanicity in the Precordillera (Lindsay et al., 1995; Reutter et al., 1996; this paper). Local development of transtensional structures within an arc-parallel fault system is most likely during such a period of stress relaxation or reversal, offering the possibility for voluminous shallow-level emplacement of magmas (e.g., Weaver et al., 1987; Tobisch and Cruden, 1995; Pitcher, 1997). In particular, transtension is most likely to develop where oblique structures intersect the main strike-slip faults, causing deflections and points of weakness. A switch from compression to extension on these cross faults could lead to the development of pull-apart basins within the zone of intersection. It is thus interesting to consider the regional structural interpretations of Salfity (1985; updated in Salfity and Gorustovich, 1998), who identified several systems of northwest- and northeast-trending lineaments that cut across the entire Andean orogen in northern Chile and Argentina, and which intersect the West Fissure zone in several places (Fig. 1). When the locations of major ore deposits in this region are superimposed on Salfity's (1985) map, a remarkable correlation is observed between major centers of mineralization and these lineament intersections (Fig. 1). The origin of these cross-orogen lineaments is

not clear, but Salfity (1985) suggests that they may date back to the Precambrian and interprets them as the boundaries of ancient basement blocks, periodically reactivated as planes of weakness during tectonism or magmatic intrusion (see also Heyl, 1972; Woodward, 1984; and Sylvester and Linke, 1993; for similar examples in North and South America). Abels and Bischoff (1999) use paleomagnetic data to support this interpretation and propose a period of large-scale, late Eocene, clockwise block rotations in the Precordillera, the northeastern edges of these blocks corresponding to the northwest-trending lineaments.

If a transtensional model for plutonism in arcs is applied to the emplacement of porphyry magmas, then, within this tectono-magmatic framework, a period of stress reversal along a major arc-parallel structural zone might provide an ideal focal mechanism, both in terms of time and space, for metalliferous intrusive activity. A transtensional model has been proposed for formation of the Chuquicamata porphyry system (Maksaev and Zentilli, 1988; Lindsay et al., 1995), and here we explore evidence for a similar control on porphyry emplacement in the Escondida region.

Geology of the Escondida, Zaldívar, and Chimborazo Porphyry Cu Deposits

Three significant porphyry copper deposits are located within 15 km of each other near latitude 24°15' S in the Chilean Precordillera (Figs. 2 and 3). In all three cases, highest grades of ore occur in supergene-enriched chalcocite and Cu oxide blankets, whereas hypogene grades are generally subeconomic (cutoff 0.3–0.4% Cu).

The Escondida mine (BHP 57.5%, Rio Tinto 30%, Mitsubishi 10%, IFC 2.5%) produced 933,000 metric tons (t) of copper (cathode and concentrate) in 1997 to rank as the largest single Cu producer in the world. In that year, proven and probable reserves stood at 2,070 million tons (Mt) of ore averaging 1.28 percent Cu (Mining Annual Review, 1997), a figure that will be substantially increased by delineation of the new Escondida Norte deposit located 6 km to the north adjacent to the Zaldívar mine (indicated sulfide resource of 676 Mt, avg 1.03% total Cu, with substantial additional inferred resources of sulfide and acid-soluble oxide Cu; Mining Journal, 1999).

Zaldívar (Placer Dome 100%) is a smaller mine than its giant neighbor, limited in part by property boundaries (Escondida Norte is contiguous with the Zaldívar orebody). Nevertheless, production in 1997 was 96,000 t of cathode copper (produced by solvent extraction and electrowinning), and proven and probable reserves stood at 267 Mt of ore, averaging 0.94 percent Cu (Placer Dome Inc. web site: http://www.placerdome.com).

The third system in this trio of porphyry deposits is the Chimborazo prospect (Minera Cyprus Chile Ltda.). Geologic resources stand at 264 Mt of mineralized rock, averaging 0.64 percent Cu (Mining Annual Review, 1997), developed as a supergene chalcocite enrichment blanket.

Escondida

A description of the geology of the Escondida deposit is the subject of a paper by Padilla (2001), but prior to this work, little has been published on the geology and metallogenesis of this giant orebody (Ojeda, 1986, 1990; Alpers and Brimhall, 1988, 1989). The deposit was discovered by Utah International and Getty Oil Company in 1981 during a regional exploration campaign along the West Fissure zone. Lowell (1991), and previously Brimhall et al. (1985) and Alpers and Brimhall (1988, 1989), described the importance of supergene processes in both the formation and discovery of the extensive, covered, chalcocite enrichment blanket that underpins the economics of this deposit.

Hypogene Cu mineralization is most closely associated with a dacitic quartz-feldspar-biotite porphyry intrusion, referred to here as the Escondida porphyry (a term that includes the Colorado Grande porphyry of some other authors). This intrusion was emplaced at 37.9 ± 1.1 Ma (2σ; U-Pb zircon dating of Richards et al., 1999) and displays potassic alteration (extensively overprinted by phyllic alteration) and hypogene Cu-Fe sulfides. The Escondida porphyry and associated mineralization were then intruded by the Rhyolitic porphyry at 34.7 ± 1.7 Ma (Richards et al., 1999). This second intrusive event appears to have introduced relatively little new Cu ore but caused extensive silicification and advanced argillic alteration (Ojeda, 1986, 1990; Alpers and Brimhall, 1988; Padilla et al., 2001). Later still, dacitic and quartz-latite porphyry dikes follow northwest-trending postmineralization faults that cut the earlier porphyries. These dikes are also weakly altered, and sericite K-Ar dates of ~31 Ma (Alpers and Brimhall, 1988) set a probable lower age limit for magmatism and hydrothermal alteration in the deposit. The broad structural framework of the deposit is controlled by two north-south faults, the Portezuelo and Panadero, which are interpreted to be strands of the West Fissure zone with dextral offsets.

Alpers and Brimhall (1988) used the K-Ar method to date alunite associated with supergene enrichment in the deposit and obtained ages of between 18 and 15 Ma, consistent with evidence from other areas in the Atacama Desert for an intense period of weathering and leaching in the early Miocene (e.g., Mortimer, 1973; Sillitoe and McKee, 1996; Tomlinson and Blanco, 1997b).

Zaldívar

Hypogene Cu mineralization at Zaldívar is largely hosted by two very similar rhyolitic quartz-feldspar porphyry bodies, the Zaldívar and Antigua porphyries, although the distribution of ore is controlled by dikes of a younger, dacitic, feldspar-biotite-quartz porphyry (the Llamo porphyry). U-Pb dating has shown that both the Antigua and Zaldívar porphyries are Paleozoic in age (290 ± 4 Ma, weighted average $^{206}Pb/^{238}U$ age; Richards et al., 1999). These felsic units can be correlated with other fault blocks of Paleozoic igneous rocks belonging to the La Tabla Formation, which crop out in the eastern part of the map area. Less altered examples of these quartz-feldspar porphyritic rocks found away from the vicinity of the mines preserve evidence for vitrophyric and eutaxitic textures, suggesting a volcanic (ignimbritic) rather than intrusive origin consistent with the occurrence of large late Paleozoic caldera structures in the Cordillera de Domeyko (e.g., the Imilac caldera; Davidson et al., 1985).

Although the Paleozoic rocks host much of the hypogene Cu inventory of the deposit, the source of this mineralization appears to be the younger Llamo porphyry, which is spatially associated with the highest grades of hypogene chalcopyrite-bornite ore (up to 0.3% Cu). Richards et al. (1999) dated this intrusion by the U-Pb (zircon) method and obtained an estimate for the age of emplacement of 38.7 ± 1.3 Ma, within error of the date obtained for the Escondida porphyry. A slightly younger $^{40}Ar/^{39}Ar$ date of 37.40 ± 0.18 Ma was also obtained for biotite from the same sample and is interpreted to reflect subsolidus persistence of the mineralizing hydrothermal system.

Similar Llamo-type porphyry dikes are found below the pit floor at the satellite Pinta Verde deposit (Fig. 3), in the adjacent Escondida Norte deposit, and at the Chimborazo prospect (see below). In addition, although the Escondida porphyry is everywhere extensively altered, there is evidence that this, too, was a biotitic porphyry (Ojeda, 1990) and might be correlative with these Llamo-type intrusions.

A major north-south fault, called the Portezuelo fault at Zaldívar but apparently not equivalent to the Portezuelo fault at Escondida, juxtaposes the Zaldívar porphyry against andesites of the Augusta Victoria Formation on the west side of the deposit. The Llamo porphyry intrudes and crosscuts the Portezuelo fault and both the Zaldívar and Antigua porphyries.

Chimborazo

The Chimborazo deposit is marked by a prominent hill of silicified and brecciated volcanic rocks of the Augusta Victoria Formation (Cerro Chimborazo), which include andesitic lavas and felsic tuffs. Although discovery of Cu mineralization at Chimborazo predates by many years the discoveries of the Escondida and Zaldívar deposits, delineation of mineable reserves at Chimborazo has not yet proven possible. Exploration work to date suggests that supergene mineralization is primarily developed in volcanic country rocks but may represent enrichment in the roof zone of a deeper porphyry system (Petersen et al., 1994, 1996). These volcanic rocks variably show potassic alteration (with weak hypogene Cu-Fe sulfide mineralization), propylitic alteration, and late advanced argillic alteration. Cerro Chimborazo itself is just one of a number of silica breccia bodies that crop out through an ~20-km^2 area of gravel cover, indicating the operation of a very large scale hydrothermal system.

Small dikes of andesitic feldspar-biotite-quartz porphyry (resembling the Llamo porphyry at Zaldívar) intrude the altered volcanic rocks on Cerro Chimborazo, and their emplacement has been dated at 38.09 ± 0.30 Ma ($^{40}Ar/^{39}Ar$ dating of biotite from sample IM154; Richards et al., 1999). A similar date was reported by Petersen et al. (1996) for a late hornblende-porphyritic diorite (38.8 ± 3.4 Ma (2σ?); K-Ar on hornblende). These dike rocks are relatively unaltered compared to the volcanic sequence and so may represent post- or synmineralization intrusions. Their age is identical to those of synmineralization intrusions at Escondida and Zaldívar, and Richards et al. (1999) have argued that this indicates that porphyry magmatism occurred during a single late Eocene (~38 Ma) event in this district.

K-Ar and $^{40}Ar/^{39}Ar$ Dating of Igneous Rocks from the Escondida District

Nine samples of the least altered, hornblende-bearing dioritic rocks from throughout the field area were selected for $^{40}Ar/^{39}Ar$ dating in order to establish the temporal framework of igneous activity within which the porphyry systems have been emplaced. The sample locations and results, along with some K-Ar dates shown in the map of Marinovic et al. (1992), are plotted in Figure 3, and the new data are listed in Tables 2 and 3.

Hornblende was separated from crushed and sieved samples by standard heavy-liquid density-separation techniques, and handpicked to >99 percent purity. Approximately 50 mg of hornblende from each sample was wrapped in Al foil and irradiated (along with splits of TCR sanidine as flux monitor) for 10 h at ~1 MW in the TRIGA research reactor, Oregon State University.

Total fusion analyses were performed at the Scottish Universities Research and Reactor Centre (SURRC), using a 20W Nd-YAG laser with an external shutter, focused through a modified petrographic microscope. Samples were fused for 2 min, and the released gases were purified for 10 min on two SAES C50 getters at 450°C. Argon isotopes were analyzed on a MAP 215 mass spectrometer with Nier-type source in static mode. The resulting analyses were corrected for blanks, ^{37}Ar decay, and neutron interferences, following the method of Singer and Pringle (1996).

Results

Hornblende-porphyritic igneous rocks are widespread throughout the map area, and distinction in terms of age, and sometimes even intrusive versus extrusive origin, is often difficult in the field where contact relationships are rarely visible. It was expected that most of the dioritic rocks sampled would be Tertiary in age, and for the most part this expectation was validated by the $^{40}Ar/^{39}Ar$ results shown in Tables 2 and 3: the majority of samples yielded dates between 38.28 ± 0.32 and 36.94 ± 0.46 Ma (2σ), which are slightly younger than K-Ar dates of 42.0 ± 4.5 and 43.9 ± 1.3 Ma for similar dioritic intrusions just outside the map area (Marinovic et al., 1992). However, one sample of dacitic hornblende porphyry (IM86) collected from the east-central part of the map area proved to be Paleozoic (267.6 ± 4.3 Ma).

Two other samples of a well-preserved hornblende gabbro intrusion (IM158, IM159) collected from the extreme southwest corner of the map area yielded Late Cretaceous dates of 76.9 ± 1.2 and 74.0 ± 2.0 Ma, consistent with a K-Ar date of 74.8 ± 2.0 Ma reported by Marinovic et al. (1992) for another nearby intrusion.

In addition to these data, Marinovic et al. (1992) also reported a date of 55.0 ± 1.4 Ma for an andesitic lava(?) in volcano-sedimentary sequences of the Augusta Victoria Formation in the northern part of the map area, and two dates of 196 ± 7 and 169 ± 6 Ma for andesitic volcanic rocks in the eastern central part of the map, corresponding presumably to the Agua Dulce Formation (although this unit is believed to be Late Triassic in age; Marinovic et al., 1992).

TABLE 2. $^{40}Ar/^{39}Ar$ Laser-Fusion Data for Hornblende from Igneous Rock Samples from the Escondida Region

Step[1]	$^{40}Ar/^{39}Ar$[2]	$^{37}Ar/^{39}Ar$[2]	$^{36}Ar/^{39}Ar$[2]	$^{40}Ar_R$ (mol)	$^{40}Ar_R$[3]	$^{40}Ar_K$[3]	$^{39}Ar_{Ca}$[3]	$^{36}Ar_{Ca}$[3]	K/Ca (%)	^{39}Ar (%)	Apparent age (Ma ± 2σ)[4]
IM46	J = 0.002769 ± 0.0000083 (1σ)		Exp. no.: jr7l0073.IHD		Total gas age = 38.26 ± 0.32 Ma						
tf1	11.246	12.226	0.015228	3.40E-14	68.5	0.01	0.82	21.20	0.040	19.2	38.36 ± 0.52
tf2	10.322	12.226	0.012274	3.00E-14	74.1	0.01	0.82	26.30	0.040	16.8	38.12 ± 0.56
tf3	10.173	11.940	0.011595	3.30E-14	75.5	0.01	0.80	27.19	0.041	18.8	38.25 ± 0.46
tf4	11.295	12.314	0.015299	4.00E-14	68.5	0.01	0.83	21.25	0.039	22.3	38.54 ± 0.46
tf5	12.040	11.209	0.017860	4.10E-14	63.4	0.01	0.75	16.57	0.043	22.9	38.03 ± 0.52
IM47	J = 0.002771 ± 0.0000083 (1σ)		Exp. no.: jr7l0074.IHD		Total gas age = 38.43 ± 0.36 Ma						
tf1	15.905	10.468	0.030960	4.80E-14	47.6	0.01	0.70	8.93	0.046	16.4	37.73 ± 0.78
tf2	11.014	7.666	0.013559	6.00E-14	69.0	0.01	0.52	14.93	0.064	20.2	37.81 ± 0.42
tf3	14.241	9.663	0.024990	6.60E-14	53.4	0.01	0.65	10.21	0.050	22.2	37.88 ± 0.50
tf4[5]	26.250	9.578	0.064020	7.30E-14	30.8	0.00	0.64	3.95	0.051	23.3	40.17 ± 1.16
tf5	17.344	10.884	0.035620	5.30E-14	44.2	0.00	0.73	8.07	0.045	17.9	38.20 ± 0.78
IM70	J = 0.002775 ± 0.0000083 (1σ)		Exp. no.: jr7l0079.IHD		Total gas age = 37.93 ± 0.32 Ma						
tf1	14.217	10.773	0.025250	6.70E-14	53.4	0.01	0.73	11.26	0.045	17.6	37.89 ± 0.62
tf2	11.314	10.210	0.015406	7.10E-14	66.8	0.01	0.69	17.50	0.048	18.8	37.70 ± 0.54
tf3	13.069	9.853	0.020970	9.70E-14	58.5	0.01	0.66	12.40	0.049	25.5	38.10 ± 0.40
tf4	10.085	10.349	0.011353	6.60E-14	74.7	0.01	0.70	24.06	0.047	17.7	37.60 ± 0.50
tf5	13.979	10.313	0.024060	7.80E-14	54.9	0.01	0.69	11.31	0.047	20.5	38.26 ± 0.48
IM79	J = 0.002777 ± 0.0000083 (1σ)		Exp. no.: jr7l0077.IHD		Total gas age = 36.89 ± 0.30 Ma						
tf1	11.008	7.490	0.013965	8.10E-14	67.8	0.01	0.50	14.16	0.065	22.5	37.20 ± 0.38
tf2	11.536	8.548	0.016348	7.00E-14	63.9	0.01	0.58	13.80	0.057	19.9	36.76 ± 0.32
tf3	14.356	7.017	0.025790	8.80E-14	50.7	0.01	0.47	7.18	0.070	25.2	36.28 ± 0.52
tf4	15.225	7.839	0.028620	5.60E-14	48.5	0.01	0.53	7.23	0.062	15.9	36.78 ± 0.54
tf5	10.246	9.510	0.011653	6.00E-14	73.6	0.01	0.64	21.55	0.051	16.5	37.64 ± 0.52
IM86	J = 0.002779 ± 0.0000083 (1σ)		Exp. no.: jr7l0076.IHD		Total gas age = 267.1 ± 1.6 Ma						
tf1	63.810	8.324	0.025250	2.50E-13	89.3	0.00	0.56	8.70	0.059	26.4	266.6 ± 1.80
tf2	60.510	7.505	0.010663	3.40E-13	95.8	0.00	0.51	18.58	0.065	34.8	270.6 ± 1.20
tf3	63.640	7.769	0.026340	3.70E-13	88.7	0.00	0.52	7.79	0.063	38.9	264.2 ± 1.40
IM90	J = 0.002755 ± 0.0000083 (1σ)		Exp. no.: jr8l0260.IHD		Total gas age = 37.26 ± 0.84 Ma						
tfa	13.693	6.587	0.023180	8.80E-14	53.7	0.01	0.44	7.50	0.074	56.4	36.36 ± 0.72
tf1	18.341	6.643	0.037590	2.00E-14	42.3	0.00	0.45	4.67	0.073	11.8	38.29 ± 1.80
tf2	15.742	6.830	0.029310	9.30E-15	48.4	0.01	0.46	6.15	0.071	5.8	37.62 ± 2.80
tf3	11.815	7.397	0.015044	9.00E-15	67.2	0.01	0.50	12.98	0.066	5.3	39.26 ± 10.88
tf4	16.782	7.083	0.031050	9.70E-15	48.6	0.01	0.48	6.02	0.069	5.6	40.29 ± 2.66
tf5	15.873	6.742	0.029420	1.30E-14	48.5	0.01	0.45	6.05	0.072	8.0	38.05 ± 2.28
tf6	19.231	7.539	0.041320	1.20E-14	39.6	0.00	0.51	4.82	0.065	7.1	37.6 ± 2.34
IM110	J = 0.002787 ± 0.0000084 (1σ)		Exp. no.: jrim110.IHD		Total gas age = 37.02 ± 0.70 Ma						
tf1[5]	88.870	10.117	0.284000	8.40E-15	6.4	0.00	0.68	0.94	0.048	6.0	28.73 ± 6.08
tf2	12.869	9.091	0.020530	6.10E-14	58.4	0.01	0.61	11.69	0.054	33.2	37.59 ± 0.70
tf3[5]	40.170	7.792	0.116430	1.50E-14	15.9	0.00	0.52	1.77	0.063	9.9	31.94 ± 3.82
tf4	14.232	9.505	0.024810	7.60E-14	53.7	0.01	0.64	10.12	0.051	40.8	38.26 ± 0.80
fs5	14.334	10.265	0.024120	5.90E-15	55.9	0.01	0.69	11.23	0.047	3.0	40.08 ± 2.04
fs6	11.147	10.628	0.013376	4.80E-15	72.0	0.01	0.72	20.98	0.046	2.4	40.18 ± 2.24
fs7	11.165	10.080	0.013522	9.10E-15	71.2	0.01	0.68	19.68	0.048	4.7	39.82 ± 1.80

TABLE 2. *(Cont.)*

Step[1]	$^{40}Ar/^{39}Ar^2$	$^{37}Ar/^{39}Ar^2$	$^{36}Ar/^{39}Ar^2$	$^{40}Ar_R$ (mol)	$^{40}Ar_R{}^3$	$^{40}Ar_K{}^3$	$^{39}Ar_{Ca}{}^3$	$^{36}Ar_{Ca}{}^3$	K/Ca (%)	^{39}Ar (%)	Apparent age (Ma ± 2s)[4]
IM158	J = 0.00279 ± 0.0000084 (1σ)		Exp. no.: jr7l0189.IHD		Total gas age = 77.05 ± 0.64Ma						
tf1	17.470	5.965	0.008863	2.20E-13	87.7	0.00	0.40	17.77	0.082	17.4	75.78 ± 0.84
tf2	20.540	5.237	0.016911	2.70E-13	77.7	0.00	0.35	8.18	0.093	21.2	78.83 ± 0.94
tf3	17.938	5.582	0.009383	2.90E-13	87.0	0.00	0.38	15.71	0.087	23.3	77.14 ± 0.78
tf4	20.720	5.927	0.019542	2.30E-13	74.4	0.00	0.40	8.01	0.082	18.7	76.24 ± 0.94
tf5	20.440	6.239	0.018217	2.40E-13	76.0	0.00	0.42	9.04	0.078	19.3	76.90 ± 1.48
IM159	J = 0.002792 ± 0.0000084 (1σ)		Exp. no.: jr7l0159.IHD		Total gas age = 73.68 ± 0.92 Ma						
tf1	25.860	5.303	0.03693	4.50E-14	59.4	0.00	0.36	3.79	0.092	21.0	76.04 ± 1.42
tf2	27.010	6.398	0.04351	4.30E-14	54.3	0.00	0.43	3.88	0.076	21.0	72.66 ± 1.82
tf3	24.530	5.670	0.03482	4.20E-14	59.9	0.00	0.38	4.30	0.086	20.3	72.75 ± 2.14
tf4	40.090	11.000	0.08694	3.90E-14	38.1	0.00	0.74	3.34	0.044	18.3	75.82 ± 1.86
tf5	40.450	10.313	0.09113	3.90E-14	35.4	0.00	0.69	2.99	0.047	19.4	71.22 ± 1.80

[1] Steps labeled either as tf for total fusion or fs for previously degassed crystals
[2] Corrected for ^{37}Ar and ^{39}Ar decay, half-lives 35.1 d and 259 yr, respectively
[3] Radiogenic (R), calcium-derived (Ca), and potassium-derived (K) argon, respectively (%)
[4] Ages calculated relative to 85G003 TCR sanidine at 27.92 Ma with $\lambda_e = 0.581 \times 10^{-10}$ a^{-1} and $\lambda_b = 4.692 \times 10^{-10}$ a^{-1}
[5] Low radiogenic ^{40}Ar content and high resultant error in calculated age, probably due to alteration; these analyses were excluded from the averaged age estimates given in Table 3

TABLE 3. Summary of $^{40}Ar/^{39}Ar$ Laser-Fusion Ages for Hornblende for Igneous Rock Samples from the Escondida Region

Sample no.	Lithology	K/Ca	Age (Ma ± 2σ)	MSWD
IM46	Hornblende diorite	0.041	38.28 ± 0.32	0.66
IM47	Hornblende diorite	0.051	37.87 ± 0.28	0.31
IM70	Hornblende diorite	0.047	37.94 ± 0.34	1.29
IM79	Porphyritic andesite dike	0.062	36.94 ± 0.46	4.20
IM90	Porphyritic dacite dike	0.072	37.01 ± 0.88	2.14
IM110	Hornblende diorite	0.050	38.25 ± 0.88	3.20
IM158	Hornblende gabbro	0.085	76.9 ± 1.2	6.56
IM159	Hornblende gabbro	0.070	74.0 ± 2.0	6.26
IM86	Dacite porphyry	0.062	267.6 ± 4.3	26.58

Note: All ages relative to USGS TCR sanidine at 27.92 Ma

Whole-Rock Geochemistry of Igneous Rocks from the Escondida District

Forty-eight samples of igneous rocks from the map area have been analyzed for major and trace element compositions by X-ray fluorescence (XRF) and inductively-coupled plasma mass spectrometer (ICP-MS) techniques. The results are reported in Table 4, grouped according to stratigraphic associations. Good agreement was obtained between analyses of the same trace elements by the ICP-MS and XRF pressed powder pellet methods, but for consistency, ICP-MS data are reported where available for trace elements and XRF (fused bead) data for major elements. Replicate analyses of international standards indicate accuracy to within 10 relative percent of the standard values for reported trace elements and to within 1 relative percent of the standard values for major elements (within 0.1 wt % of the absolute values at levels below 2 wt %).

Samples were prepared at the University of Leicester, UK, by jaw-crushing, followed by grinding in a tungsten-carbide ring mill. Laboratory experience has shown that contamination from the mill can introduce significant amounts of W (up to 400 ppm), Co (up to 80 ppm), and Ta (up to 5 ppm) when grinding felsic igneous rocks, and values for these elements are not, therefore, reported in Table 4.

Pressed powder pellets and fused glass beads were prepared and analyzed by standard XRF methods at the University of Leicester. ICP-MS analyses were conducted at the University of Saskatchewan, Canada, and involved dissolution of sample aliquots in nitric and hydrofluoric acid, dilution to a standard volume in deionized water, and analysis using a Perkin Elmer ELAN 5000, following the method of Jenner et al. (1990).

Lithological classifications are applied to the samples listed in Table 4 following the IUGS scheme of Le Maitre (1989) where possible. Many units are porphyritic, however, and these lithologies are indicated as such after a root name based on their chemical composition (for fine-grained rocks) or modal mineralogy (coarse-grained rocks).

Trace element data are presented below as spider diagrams, normalized using the average primitive mantle or C1 chondrite compositions of Sun and McDonough (1989).

TABLE 4. Major (XRF) and Trace Element (ICP-MS except where shown) Data for Igneous Rock Samples from the Escondida Region (samples are listed in stratigraphic order, starting with Paleozoic volcanic rocks)

Sample no.	IM40	IM43	IM58	IM85	IM86	ZAL2	ZAL3	IM72	IM88	IM89
Stratigraphic unit	Pz_{rp}	Pz_{ap}	Pz_{and}	Pz_{ap}	Pz_{ap}	Pz_{rp}	Pz_{rp}	Tr_{and}	Tr_{and}	Tr_{rhy}
IUGS Classification	Rhyolitic vitrophyre	Andesite (p.)	Andesitic vitrophyre	Dacite (p.)	Dacite (p.)	Rhyolitic vitrophyre (Zaldívar P.)	Rhyolitic vitrophyre (Antigua P.)	Basaltic andesite	Basaltic andesite	Rhyolitic tuff
Major elements (wt %)										
SiO_2	70.93	61.84	60.74	63.56	64.40	78.60	74.43	53.06	54.60	73.04
TiO_2	0.48	0.64	0.83	0.69	0.67	0.18	0.59	0.69	0.99	0.15
Al_2O_3	14.17	15.80	22.58	16.07	15.64	11.31	14.62	17.79	16.75	13.59
Fe_2O_3	3.53	5.83	8.11	5.66	5.33	1.42	1.72	7.99	7.56	1.01
MnO	0.07	0.10	0.03	0.10	0.10	0.02	0.02	0.16	0.14	0.03
MgO	0.63	2.88	0.64	2.41	2.27	0.20	0.34	6.10	5.97	0.49
CaO	1.20	4.10	0.97	4.25	3.66	0.06	0.07	7.55	5.97	1.13
Na_2O	3.38	2.87	1.11	3.18	3.55	1.39	1.91	2.75	3.51	1.37
K_2O	4.19	3.36	2.83	2.53	2.63	2.82	2.09	0.83	1.07	3.06
P_2O_5	0.11	0.13	0.12	0.17	0.16	0.03	0.06	0.12	0.26	0.03
LOI	1.02	1.86	1.43	1.38	1.40	2.38	3.75	2.33	2.34	2.62
Total	99.71	99.40	99.39	100.00	99.81	98.41	99.59	99.37	99.14	96.52
Trace elements (ppm)										
Cs	2.2	4.4	19	3.8	3.5	1.9	3.4	5.8	2.0	2.9
Tl	0.74	0.52	1.0	0.32	0.34	0.92	1.3	0.21	0.27	0.76
Rb	140	130	160	71	78	120	100	21	23	110
Ba	1100	540	600	670	670	690	810	250	330	660
Th	11	14	19	5.6	6.4	11	9.8	2.4	1.6	9.8
U	3.0	3.8	2.3	1.6	1.7	1.9	2.0	0.68	0.45	4.9
Nb	8.2	6.9	5.0	5.3	4.5	8.8	3.8	2.3	6.3	7.6
La	35	21	29	22	22	26	33	8.7	15	6.0
Ce	71	43	49	45	46	53	67	19	32	14
Pb	14	13	8.0	9.8	12	25	46	6.4	8.0	14
Pr	8.1	4.9	6.1	5.3	5.4	5.7	7.4	2.4	3.9	1.6
Mo	1.5	1.2	2.9	0.86	0.68	2.5	5.7	0.45	1.2	0.51
Sr	350	310	310	380	360	37	140	470	600	120
Nd	30	18	24	20	21	20	28	10	16	5.6
Sm	6.2	3.8	5.7	4.3	4.4	3.9	5.6	2.6	3.7	1.9
Zr	200	180	190	180	180	130	230	78	140	52
Hf	5.5	4.4	4.9	4.9	5.0	4.0	5.7	2.1	3.3	2.2
Eu	1.5	0.85	1.5	1.0	1.0	0.54	1.4	0.82	1.1	0.13
Sn	2.4	1.1	1.9	1.3	1.5	6.2	3.9	0.62	0.86	1.8
Sb	0.92	0.50	0.62	0.14	0.22	0.31	0.59	0.40	0.53	0.24
Gd	5.5	3.5	5.2	4.0	4.0	3.4	4.7	2.6	3.5	2.2
Tb	0.81	0.58	0.68	0.60	0.58	0.55	0.72	0.40	0.54	0.49
Dy	5.2	3.6	3.9	3.8	3.8	3.6	4.6	2.5	3.5	3.4
Li	14	32	47	30	23	2.6	5.0	38	12	7.4
Y	30	21	20	22	23	23	27	16	19	22
Ho	1.1	0.75	0.77	0.80	0.78	0.79	0.98	0.55	0.71	0.74
Er	3.1	2.1	2.1	2.3	2.3	2.4	2.7	1.5	2.0	2.2
Tm	0.49	0.33	0.33	0.35	0.34	0.41	0.43	0.23	0.30	0.35
Yb	3.3	2.3	2.2	2.1	2.2	2.8	2.9	1.6	1.9	2.3
Lu	0.47	0.31	0.32	0.35	0.36	0.42	0.44	0.21	0.28	0.33
Sc	10	19	70	16	14	6.0	12	30	24	6.7
V	34	140	290	110	98	5.5	33	220	170	8.8
Cr	0.88	15	140	10	10	0.45	3.2	88	190	5.6
Ni	1.2	14	26	9.9	9.8	0.76	1.1	62	100	2.2
Cu	4.3	59	13	50	47	990	260	79	52	8.5
Zn	36	59	30	57	53	8.0	29	60	72	18
Cd	0.04	0.10	0.03	0.11	0.13	0.00	0.03	0.22	0.16	0.16
As(XRF)	8	5	12	8	5	5	7	6	5	5
Ga(XRF)	17	17	19	18	17	14	17	17	18	17
S(XRF)	270	110	120	110	110	17000	6600	110	2400	9300
Eu_n/Eu^*	0.77	0.71	0.86	0.74	0.75	0.45	0.81	0.98	0.93	0.20
La_n/Yb_n	7.7	6.6	9.4	7.3	7.2	6.6	8.1	4.0	5.7	1.9

TABLE 4. *(Cont.)*

Sample no.	IM95	IM96	IM98	IM122	IM156	IM158	IM159	IM128	IM8	IM10
Stratigraphic unit	Tr_{rhy}	Tr_{and}	Tr_{rhy}	Tr_{rhy}	K_g	K_g	K_g	T_{and}	T_{di}	T_{di}
IUGS Classification	Rhyolitic tuff	Basaltic andesite	Rhyolitic vitrophyre	Rhyolitic vitrophyre	Hbl gabbro	Hbl gabbro	Hbl gabbro	Basaltic andesite	Diorite (p.)	Diorite
Major elements (wt %)										
SiO_2	74.23	52.82	74.34	73.42	44.76	45.63	45.28	54.46	58.25	59.69
TiO_2	0.15	0.97	0.09	0.08	1.13	1.74	1.87	0.82	0.74	0.77
Al_2O_3	13.65	17.60	12.69	12.26	18.90	17.55	19.85	17.69	16.95	17.27
Fe_2O_3	0.93	8.10	0.51	0.52	6.95	11.32	11.56	7.34	5.41	5.54
MnO	0.06	0.15	0.06	0.07	0.11	0.08	0.13	0.11	0.10	0.09
MgO	0.42	6.34	0.21	0.14	7.44	6.18	5.35	3.49	2.58	2.95
CaO	2.23	6.86	0.65	0.45	13.13	8.18	10.71	7.91	5.97	5.77
Na_2O	1.47	2.88	4.60	4.77	1.50	3.38	2.82	2.88	3.64	3.37
K_2O	2.41	0.66	3.02	3.02	1.79	1.62	0.96	1.54	1.93	2.03
P_2O_5	0.04	0.31	0.02	0.02	0.15	0.60	0.23	0.27	0.28	0.27
LOI	3.72	2.62	3.70	3.75	3.50	2.84	0.77	2.36	0.29	1.49
Total	99.33	99.31	99.90	98.51	99.34	99.12	99.51	98.86	96.15	99.24
Trace elements (ppm)										
Cs	1.9	3.9	23	13	4.5	0.93	0.87	2.6	2.2	0.63
Tl	0.98	0.17	2.3	2.5	0.44	0.21	0.01	0.20	0.18	0.22
Rb	100	19	200	200	56	54	25	46	52	54
Ba	160	240	180	190	150	260	180	530	660	610
Th	8.4	1.9	9.0	9.0	1.3	2.8	0.97	4.0	4.6	5.1
U	3.7	0.49	4.3	4.1	0.27	0.50	0.28	1.0	0.87	1.3
Nb	6.1	6.7	4.9	3.4	11	30	7.4	6.8	6.5	7.8
La	7.0	16	6.8	6.6	8.0	19	10	20	23	22
Ce	16	36	16	15	18	43	20	40	47	46
Pb	170	8.2	19	22	0.88	1.0	1.8	8.2	9.8	9.9
Pr	2.0	4.4	1.7	1.8	2.3	5.6	2.5	4.8	5.5	5.3
Mo	2.0	0.68	1.1	1.2	0.45	0.31	0.46	1.4	1.0	1.6
Sr	54	680	174	64	540	890	900	590	650	690
Nd	6.6	18	5.9	5.5	10	24	11	19	22	21
Sm	2.0	4.1	1.6	1.7	2.6	5.3	2.6	4.1	4.1	4.0
Zr	49	150	38	37	71	186	57	130	170	150
Hf	1.9	3.3	1.7	1.7	2.3	4.8	1.5	3.2	4.3	4.0
Eu	0.17	1.2	0.13	0.12	0.96	1.5	1.3	1.2	1.2	1.1
Sn	1.6	1.1	1.8	1.6	2.1	1.3	0.74	1.0	0.95	0.98
Sb	0.33	0.83	0.48	0.32	0.22	0.11	0.05	1.2	0.10	0.10
Gd	2.1	3.8	1.8	1.8	2.6	5.3	2.5	3.5	3.5	3.2
Tb	0.45	0.58	0.37	0.34	0.39	0.72	0.35	0.52	0.41	0.40
Dy	3.0	3.6	2.5	2.4	2.3	4.5	2.1	3.1	2.6	2.4
Li	28	35	4.9	4.6	34	32	12	22	13	27
Y	19	20	17	16	12	24	12	17	15	14
Ho	0.66	0.73	0.55	0.53	0.45	0.85	0.41	0.59	0.50	0.46
Er	1.9	2.0	1.7	1.6	1.2	2.3	1.1	1.6	1.4	1.3
Tm	0.30	0.30	0.26	0.26	0.16	0.33	0.15	0.24	0.21	0.19
Yb	2.0	1.8	1.8	1.7	0.96	2.2	0.92	1.6	1.3	1.2
Lu	0.28	0.27	0.25	0.25	0.15	0.34	0.13	0.23	0.20	0.19
Sc	6.1	25	3.7	4.2	42	21	21	17	12	11
V	14	190	1.2	1.1	170	170	250	160	110	100
Cr	5.8	150	0.60	0.06	310	120	12	11	16	18
Ni	4.5	115	0.71	0.28	110	62	17	14	14	16
Cu	10	45	1.2	1.3	17	4.8	19	57	63	53
Zn	180	62	17	17	33	30	31	79	73	58
Cd	2.1	0.43	0.03	0.00	0.07	0.00	0.05	0.07	0.08	0.06
As(XRF)	0	9	2	3	3	3	3	4	2	2
Ga(XRF)	17	19	15	14	17	21	22	18	20	20
S(XRF)	10000	9800	110	150	140	110	850	110	110	110
Eu_n/Eu^*	0.25	0.92	0.23	0.22	1.1	0.88	1.5	0.98	0.95	0.95
La_n/Yb_n	2.6	6.4	2.7	2.9	6.0	6.3	7.9	9.1	13	13

TABLE 4. *(Cont.)*

Sample no.	IM14	IM45	IM46	IM47	IM50	IM52	IM53	IM55	IM59	IM60
Stratigraphic unit	T_{di}	T_{di}	T_{di}	T_{di}	T_{di}	T_{di}	T_{di}	T_{di}	T_{di}	T_{di}
IUGS Classification	Diorite	Diorite	Diorite (p.)	Diorite (p.)	Diorite (p.)	Diorite (p.)	Diorite (p.)	Diorite (p.)	Diorite	Diorite (p.)
Major elements (wt %)										
SiO_2	59.87	58.52	61.44	57.79	58.12	57.29	56.19	57.75	57.23	57.55
TiO_2	0.88	0.86	0.66	0.87	0.94	0.90	0.84	0.87	0.89	0.79
Al_2O_3	18.47	17.56	16.68	18.49	17.81	17.53	17.98	17.67	18.12	17.72
Fe_2O_3	6.35	5.65	4.76	6.42	6.40	6.32	6.56	6.34	6.47	6.36
MnO	0.12	0.11	0.09	0.11	0.11	0.10	0.13	0.08	0.12	0.12
MgO	2.88	3.10	2.49	3.41	3.76	3.77	3.48	3.55	3.87	3.41
CaO	6.49	6.10	4.46	6.60	6.81	6.58	6.40	6.38	7.02	6.34
Na_2O	3.65	3.69	3.86	3.43	3.27	3.34	3.50	3.21	3.32	3.23
K_2O	1.30	1.62	2.22	1.45	1.41	1.48	1.47	1.85	1.14	1.63
P_2O_5	0.30	0.31	0.24	0.35	0.30	0.30	0.33	0.31	0.29	0.29
LOI	0.20	1.58	1.81	1.05	1.17	1.22	1.59	1.71	1.25	2.04
Total	100.51	99.09	98.71	99.98	100.11	98.84	98.47	99.74	99.72	99.47
Trace elements (ppm)										
Cs	1.3	1.2	1.1	0.49	0.28	0.46	0.50	0.58	0.73	1.2
Tl	0.17	0.25	0.32	0.15	0.14	0.15	0.27	0.13	0.18	0.15
Rb	35	46	71	34	34	42	36	36	27	46
Ba	550	570	700	530	550	550	530	650	570	560
Th	3.8	4.0	5.9	2.7	3.9	3.8	3.3	4.3	2.6	4.2
U	0.63	0.78	1.3	0.63	1.0	0.96	0.66	0.99	0.55	1.0
Nb	6.0	7.9	5.9	8.0	7.0	7.0	7.5	8.4	6.5	6.9
La	20	22	23	20	21	21	21	22	19	20
Ce	42	45	45	42	42	42	42	44	40	41
Pb	8.3	6.7	5.3	6.2	6.8	6.9	8.6	5.1	12.4	9.9
Pr	5.0	5.3	5.2	5.0	5.0	4.9	5.1	5.3	4.7	5.0
Mo	1.2	0.61	0.92	1.3	1.2	1.6	1.2	1.4	0.63	1.8
Sr	680	860	640	720	690	770	810	670	810	730
Nd	20	21	20	21	20	20	20	20	19	20
Sm	4.1	4.1	3.6	4.1	3.8	3.9	4.1	4.0	3.9	3.9
Zr	140	160	170	140	140	130	150	150	130	140
Hf	3.8	4.0	3.9	3.3	3.2	3.1	3.6	3.9	3.4	3.7
Eu	1.3	1.2	0.97	1.2	1.2	1.1	1.2	1.2	1.2	1.2
Sn	1.0	0.88	0.88	0.90	1.1	0.98	0.96	0.85	0.81	0.74
Sb	0.09	0.06	0.26	0.06	0.22	0.17	0.44	0.42	0.16	0.21
Gd	3.5	3.3	2.9	3.3	3.2	3.3	3.3	3.4	3.2	3.4
Tb	0.49	0.41	0.40	0.45	0.44	0.45	0.47	0.47	0.42	0.44
Dy	2.9	2.3	2.3	2.7	2.5	2.5	2.5	2.6	2.5	2.6
Li	16	20	15	13	9.3	14	16	14	11	19
Y	17	14	14	15	14	14	16	15	15	16
Ho	0.58	0.45	0.44	0.51	0.46	0.46	0.54	0.51	0.49	0.52
Er	1.5	1.2	1.2	1.4	1.2	1.2	1.5	1.4	1.3	1.4
Tm	0.22	0.17	0.19	0.19	0.18	0.19	0.22	0.19	0.18	0.21
Yb	1.5	1.1	1.1	1.3	1.1	1.1	1.5	1.3	1.2	1.4
Lu	0.22	0.17	0.17	0.17	0.16	0.16	0.20	0.20	0.17	0.21
Sc	12	12	10	14	17	16	14	16	16	15
V	120	110	100	130	170	150	140	150	140	150
Cr	4.2	18	11	16	42	40	5.5	28	27	11
Ni	4.5	15	11	13	22	22	13	18	18	12
Cu	35	48	48	47	21	21	63	6.1	46	75
Zn	76	82	37	76	80	75	99	32	93	82
Cd	0.04	0.02	0.08	0.16	0.15	0.12	0.08	0.09	0.04	0.10
As(XRF)	2	5	7	3	2	7	15	22	4	2
Ga(XRF)	24	20	18	22	20	20	22	20	21	21
S(XRF)	110	1300	3300	110	120	150	110	110	530	460
Eu_n/Eu^*	1.0	0.96	0.92	1.0	1.0	0.97	1.0	1.0	1.0	0.98
La_n/Yb_n	9.6	15	14	11	14	13	10	12	12	11

TABLE 4. *(Cont.)*

Sample no.	IM61	IM62	IM68	IM69	IM70	IM79	IM81	IM90	IM110	IM116
Stratigraphic unit	T_{di}	T_{di}	T_{di}	T_{di}	T_{di}	T_{di}	T_{di}	T_{di}	T_{di}	T_{di}
IUGS Classification	Diorite (p.)	Diorite	Diorite (p.)	Diorite	Diorite (p.)	Andesite dike (p.)	Diorite (p.)	Dacite dike (p.)	Diorite (p.)	Dacite (p.)
Major elements (wt %)										
SiO_2	54.62	59.12	58.77	56.64	59.23	62.82	55.15	63.12	57.89	65.19
TiO_2	0.96	0.76	0.91	0.95	0.70	0.59	0.91	0.60	0.76	0.56
Al_2O_3	18.01	17.98	18.01	17.87	17.49	16.39	18.45	17.40	16.85	16.21
Fe_2O_3	6.83	6.00	6.11	6.73	5.68	3.78	6.10	3.67	5.84	4.03
MnO	0.12	0.12	0.11	0.12	0.11	0.10	0.12	0.07	0.10	0.10
MgO	4.57	2.94	3.46	4.11	2.75	1.56	3.42	1.76	3.37	1.98
CaO	6.76	6.42	6.72	7.45	5.72	4.14	7.76	4.18	5.86	3.61
Na_2O	3.46	3.77	3.51	3.17	3.50	3.95	3.33	4.58	3.17	3.75
K_2O	1.21	1.56	1.49	1.53	1.84	2.63	1.11	2.25	2.59	3.34
P_2O_5	0.30	0.29	0.30	0.27	0.27	0.24	0.31	0.24	0.24	0.19
LOI	2.65	0.13	1.11	0.31	1.72	1.21	2.22	1.27	1.51	1.42
Total	99.49	99.08	100.51	99.15	99.01	97.41	98.88	99.14	98.17	100.39
Trace elements (ppm)										
Cs	0.59	1.7	0.46	1.6	0.65	2.2	0.74	0.85	6.5	4.6
Tl	0.11	0.10	0.12	0.11	0.15	0.36	0.14	0.24	0.34	0.58
Rb	29	46	38	46	47	75	24	50	100	130
Ba	440	580	550	550	620	760	550	750	580	730
Th	1.9	3.4	3.6	3.9	4.1	5.8	2.0	3.5	12	13
U	0.45	0.78	0.91	0.87	0.84	1.4	0.46	1.0	3.4	2.8
Nb	6.0	6.4	5.6	8.0	7.8	6.0	7.2	5.7	9.0	8.6
La	16	20	20	21	22	24	19	22	24	26
Ce	36	41	41	42	45	47	41	45	49	51
Pb	7.9	9.4	12.5	8.5	7.7	10	7.6	9.6	13	16
Pr	4.6	4.8	4.9	5.0	5.3	5.3	5.1	5.2	5.6	5.7
Mo	1.5	1.9	1.7	1.6	0.58	1.2	0.80	0.47	1.4	0.99
Sr	890	730	720	700	600	680	840	790	530	530
Nd	19	19	19	21	20	20	21	20	22	21
Sm	3.9	3.7	3.8	4.3	3.9	3.5	4.1	3.5	4.4	3.8
Zr	100	140	130	160	170	150	140	160	190	180
Hf	2.8	3.4	3.2	4.1	4.9	3.5	3.4	3.9	5.2	4.8
Eu	1.2	1.1	1.2	1.2	1.1	0.98	1.2	0.97	1.1	0.97
Sn	0.78	0.88	1.0	0.91	0.79	0.85	1.0	0.88	0.86	0.81
Sb	0.17	0.04	0.09	0.04	0.08	0.04	2.0	0.51	0.55	0.46
Gd	3.4	3.2	3.0	3.7	3.2	2.4	3.2	2.5	3.7	3.1
Tb	0.43	0.40	0.42	0.49	0.42	0.33	0.39	0.26	0.49	0.38
Dy	2.6	2.5	2.3	2.9	2.5	1.7	2.2	1.5	3.0	2.4
Li	18	17	13	14	21	14	46	16	23	22
Y	14	15	13	17	15	11	13	9.5	18	15
Ho	0.50	0.48	0.44	0.56	0.51	0.34	0.42	0.27	0.58	0.46
Er	1.3	1.3	1.2	1.5	1.3	0.86	1.1	0.73	1.6	1.3
Tm	0.19	0.19	0.17	0.22	0.21	0.13	0.16	0.09	0.24	0.19
Yb	1.12	1.15	1.05	1.37	1.39	0.78	0.97	0.60	1.5	1.3
Lu	0.17	0.18	0.15	0.22	0.24	0.12	0.14	0.10	0.24	0.20
Sc	20	11	16	19	11	6.9	15	6.9	14	8.9
V	200	110	150	150	100	72	140	73	130	82
Cr	45	8.1	48	30	15	5.0	55	8.9	17	11
Ni	30	9.3	24	21	11	4.5	27	10	15	8.9
Cu	55	43	22	60	60	33	80	24	63	51
Zn	79	71	73	80	63	61	73	80	69	61
Cd	0.26	0.05	0.18	0.06	0.07	0.24	0.06	0.19	0.15	0.22
As(XRF)	8	1	5	5	7	4	8	5	7	3
Ga(XRF)	22	21	21	18	21	21	22	23	18	17
S(XRF)	120	110	110	110	110	180	110	1300	110	430
Eu_n/Eu^*	1.0	0.96	1.0	0.95	0.97	1.0	0.98	1.0	0.84	0.87
La_n/Yb_n	11	12	14	11	12	22	14	27	11	14

TABLE 4. *(Cont.)*

Sample no.	IM119	IM143	IM150	IM151	IM154	ESC1	ESC3	ZAL1
Stratigraphic unit	T_{di}	T_{di}	T_{di}	T_{di}	T_{bfp}	T_{qfp}	T_{qfp}	T_{bfp}
IUGS Classification	Dacite (p.)	Diorite (p.)	Diorite	Diorite dike (p.)	Andesite dike (p.)	Rhyolitic QFP (Rhyolitic P.)	Dacitic QFP (Escondida P.)	Dacitic QFP (Llamo P.)
Major elements (wt %)								
SiO_2	64.79	61.33	55.57	60.66	60.48	78.57	66.15	67.68
TiO_2	0.47	0.71	0.88	0.59	0.69	0.35	0.49	0.53
Al_2O_3	16.97	16.60	18.85	16.79	17.54	12.16	17.38	18.59
Fe_2O_3	2.87	5.52	7.60	4.91	4.67	1.28	3.13	1.79
MnO	0.05	0.08	0.14	0.12	0.08	0.02	0.04	0.02
MgO	1.22	2.88	3.96	2.22	3.86	0.40	1.19	0.46
CaO	3.88	4.92	7.57	5.46	2.55	0.02	2.52	0.85
Na_2O	4.20	3.28	2.97	3.23	3.26	0.18	5.14	3.20
K_2O	3.04	2.91	1.48	2.53	2.62	3.17	2.13	2.61
P_2O_5	0.21	0.21	0.27	0.39	0.29	0.05	0.21	0.18
LOI	1.21	0.69	-0.13	2.07	3.04	3.14	0.84	3.15
Total	98.91	99.12	99.17	98.98	99.08	99.33	99.21	99.05
Trace elements (ppm)								
Cs	3.0	3.5	1.6	4.3	11	2.2	1.4	6.4
Tl	0.53	0.42	0.07	0.40	0.98	1.8	0.41	1.3
Rb	84	100	44	77	74	140	52	110
Ba	860	720	520	1500	860	650	720	820
Th	3.6	12	3.6	9.3	5.8	3.7	3.7	6.1
U	1.6	2.9	0.91	2.8	1.9	1.2	0.73	2.6
Nb	4.6	10	7.6	11	8.4	1.5	6.7	9.8
La	21	25	19	45	21	21	15	24
Ce	41	50	39	87	41	39	32	48
Pb	12	13	6.6	16	33	12	13	18
Pr	4.7	5.9	4.8	9.8	4.6	4.5	3.8	5.3
Mo	1.3	1.7	1.2	0.51	1.7	3.0	7.3	6.3
Sr	920	460	640	1100	480	160	720	460
Nd	18	22	19	38	18	16	15	20
Sm	3.0	4.7	4.2	6.7	3.1	2.8	2.9	3.5
Zr	130	190	130	180	140	130	140	150
Hf	3.3	5.1	3.8	4.7	3.2	3.4	3.6	3.6
Eu	0.87	1.0	1.2	1.9	0.95	0.78	0.79	1.0
Sn	0.69	1.4	0.89	0.87	1.1	1.2	1.1	1.8
Sb	1.4	0.09	0.18	0.11	1.1	0.62	0.07	0.15
Gd	2.0	3.9	3.6	4.8	2.4	1.6	1.9	3.3
Tb	0.24	0.54	0.50	0.56	0.33	0.18	0.24	0.46
Dy	1.3	3.4	3.1	3.0	1.8	0.97	1.3	2.3
Li	18	21	14	32	22	2.4	8.6	8.9
Y	7.8	20	18	18	11	5.4	8.5	11
Ho	0.23	0.67	0.61	0.57	0.36	0.18	0.25	0.41
Er	0.55	1.9	1.7	1.5	0.91	0.49	0.69	1.0
Tm	0.09	0.29	0.26	0.21	0.14	0.07	0.10	0.13
Yb	0.53	1.9	1.6	1.4	0.96	0.49	0.59	0.86
Lu	0.08	0.30	0.27	0.22	0.13	0.08	0.10	0.12
Sc	5.2	12	17	7.6	10	3.9	5.8	6.4
V	54	100	150	89	87	26	54	54
Cr	6.3	13	12	2.4	5.4	1.7	5.7	5.0
Ni	4.5	12	13	4.7	5.7	0.45	4.8	2.2
Cu	32	31	53	28	66	47	690	1300
Zn	56	43	74	71	110	20	70	50
Cd	0.11	0.06	0.09	0.07	1.1	0.03	0.06	0.07
As(XRF)	15	0	5	38	5	7	3	7
Ga(XRF)	20	20	22	21	21	17	22	21
S(XRF)	1600	190	110	220	3200	40000	1100	200
Eu_n/Eu^*	1.1	0.73	0.95	1.0	1.1	1.1	1.0	0.94
La_n/Yb_n	29	9.6	8.3	24	16	30	19	20

Notes: Lithological classifications based on IUGS scheme of Le Maitre (1989); accuracy is estimated to be within 10 relative percent for trace elements and to within 1 relative percent for major elements (± 0.1 wt % at levels below 2 wt %); $Eu_n/Eu^* = Eu_n/\sqrt{Sm_n \times Gd_n}$; La_n/Yb_n = C1 normalization values of Sun and McDonough (1989)

Abbreviations: Stratigraphic labels as defined in Figure 3; Hbl = hornblende; p. = porphyritic; P. = porphyry; QFP = quartz-feldspar porphyry

Petrologic and Geochemical Synthesis of Stratigraphic Units

Permo-Carboniferous (La Tabla Formation)

The oldest rocks occurring in the map area are Permo-Carboniferous extrusive and intrusive lithologies of the Cordillera de Domeyko, assigned to the La Tabla Formation by Marinovic et al. (1992). These crystalline rocks appear to constitute the basement throughout the map area and crop out as fault-bounded massifs to the east of the West Fissure zone (Imilac block). The U-Pb dating results of Richards et al. (1999) indicate that the Zaldívar range of hills also belongs to this sequence.

La Tabla Formation lithologies in the map area are dominated by areally extensive quartz-feldspar porphyritic vitrophyre units, showing little macroscopic structure and rarely showing nonfaulted contact relationships with other units. In thin section, these rocks are characterized by abundant phenocrysts of quartz and feldspar (typically <5 mm in size) and lesser mafic minerals (chloritic pseudomorphs after biotite or hornblende, reflecting widespread propylitic alteration). Feldspars are extensively saussuritized, but relict plagioclase twinning can be observed locally. Quartz phenocrysts frequently show deep embayments (hourglass inclusions) and large melt inclusions, suggestive of undercooling and dendritic growth (Lowenstern, 1995). The matrix appears in all cases to have been glass but is now devitrified and locally spherulitic. Relict flow banding is preserved in many samples, and faint remnants of a eutaxitic texture are rarely observed. Given this evidence for an originally glassy or pumiceous matrix and the large areal extent of this rock type, a volcanic (ignimbritic) origin seems more likely than crystallization as subvolcanic intrusions. This interpretation is supported by the occurrence at E495400 N7325200 in the Zaldívar range of a small outcrop of sandy limestone overlying the vitrophyric sequence. This sedimentary rock is not hornfelsed and no unconformity is evident, suggesting that it concordantly overlies the vitrophyre unit, rather than having been intruded by it.

More mafic, hornblende-porphyritic dacites form steep hills near E501000 N7330000 (samples IM85 and IM86). Although superficially similar to the abundant Tertiary-age hornblende-porphyritic intrusions that crop out in the area, these units are characterized by fine-grained, devitrified matrices, suggesting a volcanic origin. They are also closely associated with minor sedimentary units (sandy or silty carbonate rocks) that show no contact metamorphic effects. Hornblende from sample IM86 yielded a $^{40}Ar/^{39}Ar$ date of 267.6 ± 4.3 Ma (Table 3), confirming its late Paleozoic age.

Four samples of vitrophyric rocks have been analyzed chemically, but three of these samples are highly altered (IM58, ZAL2, and ZAL3). The major element composition of the remaining sample, IM40, indicates a metaluminous (aluminum saturation index (ASI) < 1), high K, rhyolitic affinity. Three samples of andesitic to dacitic porphyritic volcanic rocks (IM43, IM85, IM86) share these characteristics, straddling the high to medium K boundary at their respective SiO_2 concentrations.

Trace element compositions for the seven samples of Paleozoic volcanic rocks are compared in Figure 4. Strong negative anomalies for Nb and Ti and positive anomalies for Pb and Sb (Fig. 4A) are characteristic of arc magmas, and, when combined with their major element compositions, support an I-type calc-alkaline magmatic affinity (Chappell and White, 1974). Rare earth element (REE) patterns are consistent with this classification, being characterized by light REE enrichment but relatively flat patterns for the middle and heavy REE. Slight to moderate negative Eu anomalies, combined with the flat middle to heavy REE patterns, attest to plagioclase feldspar fractionation during differentiation of these magmas.

Late Triassic (Agua Dulce Formation)

The early Mesozoic era marked the start of the Andean orogenic cycle and the breakup of Gondwana (Table 1). Arc magmatism flared in the La Negra belt near the present-day coast, but felsic and intermediate volcanism was also widespread in the back-arc region. Volcanic lithologies in the map area are characterized by subdued topographic signatures, and these units may underlie large areas of the gravel-covered pediment to the east of the West Fissure zone. Two whole-rock K-Ar dates of 196 ± 7 and 169 ± 6 Ma (Marinovic et al., 1992) are reported in the east-central part of the map area where low hills of andesitic and rhyolitic volcanic rocks crop out. Although Marinovic et al. (1992) identified these sequences as belonging to the Paleozoic La Tabla Formation, they are here correlated with the Agua Dulce Formation. The radiometric dates, which at face value suggest a Jurassic age for the volcanic rocks, may have been disturbed by later propylitic alteration (a common problem with whole-rock K-Ar dating). The boundary between the La Tabla and Agua Dulce volcanic sequences is not clear, however, and the fault-bounded contact shown in Figure 3 near E501000 is considered conjectural. Equally, the western limit of the Agua Dulce Formation in the southern half of the map area near E497000 is poorly constrained.

The andesitic volcanic rocks are porphyritic, with altered hornblende, clinopyroxene, and saussuritized plagioclase phenocrysts set in a fine-grained, sometimes trachytic, matrix. At E496900 N7326800 outcrops of carbonate-altered amygdaloidal andesite occur, but macroscopic volcanic features are otherwise not preserved. It is possible that these amygdaloidal flows correlate with similar flows found at the base of the Augusta Victoria Formation (near E488000 N7341000), but definitive correlation of these isolated outcrops is difficult.

Rhyolitic rocks contain phenocrysts of quartz, feldspar (plagioclase and lesser K feldspar), and locally minor biotite, set in a glassy matrix (usually devitrified). Some samples preserve eutaxitic textures, indicating a pyroclastic origin (e.g., IM89, IM95), whereas others preserve flow banding or the original glassy matrix and may have been formed in flow-dome complexes (e.g., IM98, IM122). These rocks tend to weather as low, scree-covered hills and ridges lacking undisturbed outcrop.

A large area of low-lying ground with sparse outcrops of andesitic and rhyolitic volcanic rocks occurs in the northern part of the map area near E490000. Following Marinovic et al. (1992), this sequence is here assigned to the Agua Dulce Formation. No volcanic structures were observed in this sequence, but the andesitic rocks are strongly oxidized to purplish colors near their western unconformable contact with an overlying Jurassic conglomerate, suggesting a period of subaerial weathering.

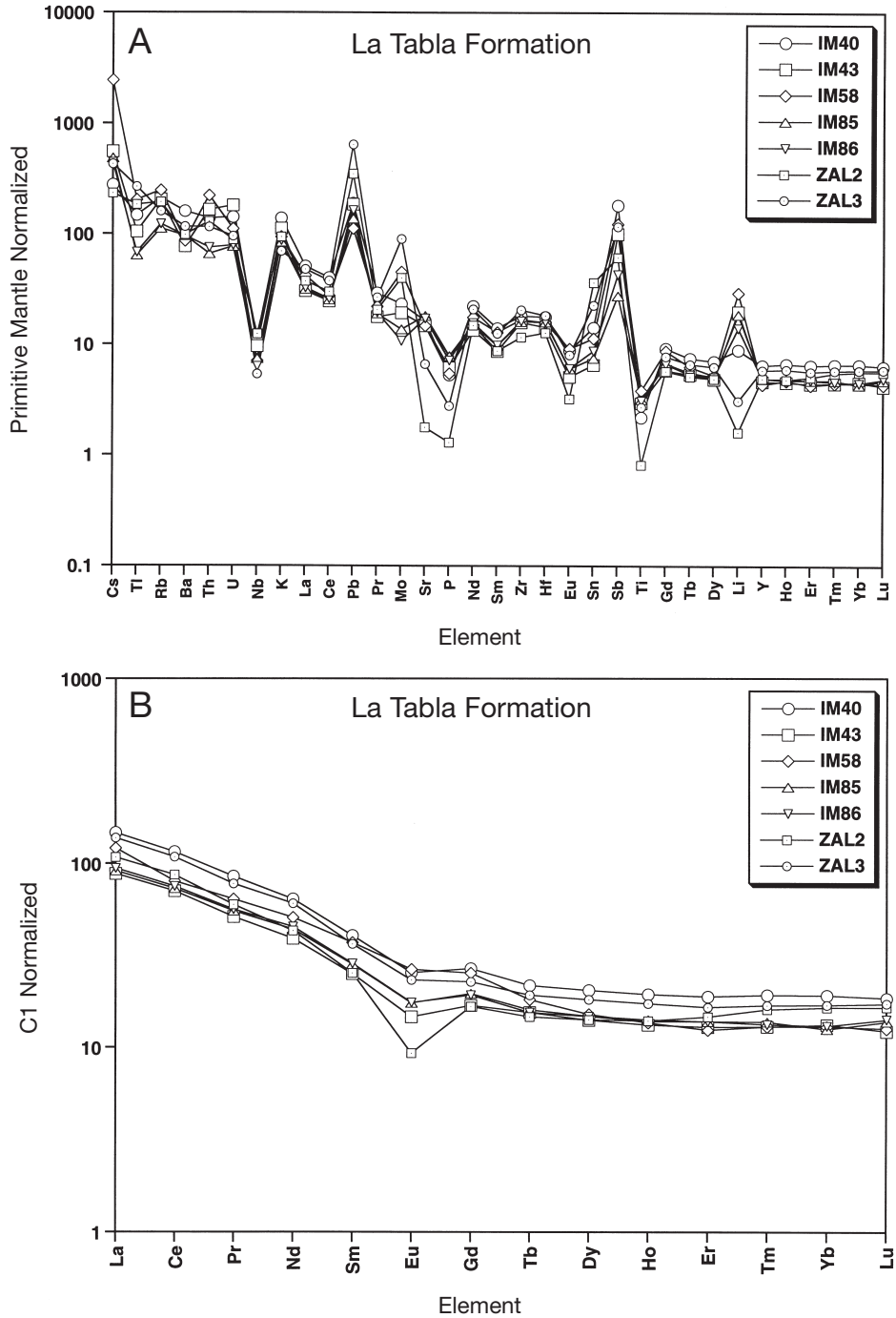

FIG. 4. Normalized trace element (A) and REE (B) diagrams for samples of Paleozoic (La Tabla Formation) intermediate to felsic volcanic rocks. The trace element data reveal arclike patterns, and Eu depletions indicate feldspar fractionation from relatively dry magmas. Normalization values of Sun and McDonough (1989).

Geochemically, the andesitic and rhyolitic volcanic rocks yield contrasting signatures, suggestive either of extreme fractionation effects or differing sources. The andesites (samples IM72, IM88, IM96) are characterized by arclike, incompatible element-enriched compositions (Fig. 5A), with strong negative anomalies at Nb and Ti and positive anomalies at Pb, Sb, and Li; REE patterns show mild, uniform light REE enrichment (Fig. 5B). In contrast, the rhyolites (samples IM89, IM95, IM98, IM122) are further enriched in the incompatible elements (particularly U and K, as well as Pb and Sb) but show depletions in some cases to below primitive mantle values in P, Eu, and Ti (Fig. 5A). The contrast between the geochemistry of these rock types is most clearly shown by their REE patterns, in which the rhyolites display only weak light REE enrichment, plus a strong negative Eu anomaly (Fig. 5B).

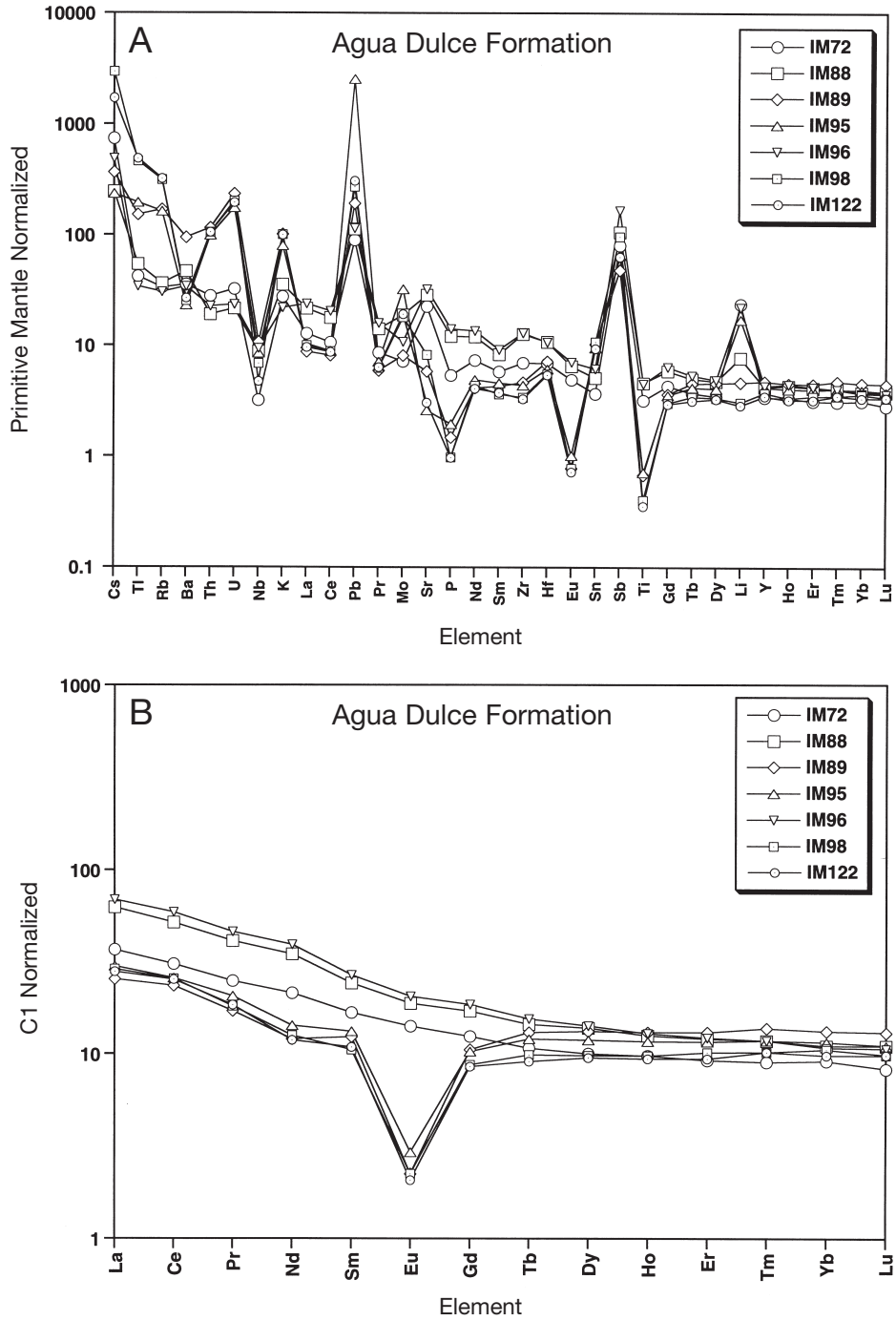

FIG. 5. Normalized trace element (A) and REE (B) diagrams for samples of Late Triassic (Agua Dulce Formation) andesitic and rhyolitic volcanic rocks. The andesites are characterized by normal arclike signatures, whereas the rhyolitic rocks show greater degrees of incompatible element enrichment and strong depletions in P, Eu, and Ti. See text for discussion. Normalization values of Sun and McDonough (1989).

Given that some of the rhyolites are preserved as obsidians with a relatively low crystal content (<10% by volume in one sample), it seems unlikely that these melts have fractionated extensively (i.e., they were quenched from close to their liquidus temperatures). Thus, their compositions are probably derived from melting a crustal source rather than by fractionation from coexisting andesitic magmas (Pichler and Zeil, 1972; Hildreth, 1981; de Silva, 1989). Magmatic underplating or voluminous intrusion of arc magmas may have caused localized melting of felsic crustal materials to give rise to this bimodal volcanism (e.g., Harmon et al., 1984; Pitcher, 1997).

Jurassic-Cretaceous (El Profeta and Santa Ana Formations)

Large areas of Jurassic-Cretaceous-age sedimentary and intercalated volcanic rocks crop out in the southwestern and northwestern parts of the map area, which are believed to

have been deposited in a subsiding back-arc basin (Table 1). These rocks form an apparently continuous sequence that is subdivided into the older El Profeta and younger Santa Ana Formations, based on a change from dominantly calcareous to dominantly arenaceous lithologies.

The base of the El Profeta Formation is well exposed in the north between N7340000 to N7350000, where a rubbly conglomerate horizon unconformably overlies oxidized andesites of the Agua Dulce Formation. This contact marks a catastrophic flooding event, and ammonites and other marine fossils are found in abundance in the directly overlying silty carbonate rocks. Fossiliferous micritic limestones, limestone breccias, and sandy and/or silty lenses characterize the ensuing sequence, which may exceed 1 km in thickness in the northern area. A single basaltic andesite lava flow is intercalated with the sediments between N7341000 and N7347500, near E490000. The lava is little altered and consists of interlocking plagioclase, clinopyroxene (locally subophitic), biotite, and interstitial glass (now devitrified).

The Santa Ana Formation is characterized by orange- and yellow-weathering sandstones and siltstones, subordinate silty carbonate horizons, and thin rhyolitic and andesitic volcanic layers. A boundary between the Santa Ana and El Profeta Formations has not been mapped in this study, but in the northern area it probably occurs near E489000 N7343000, where a prominent north-trending ridge of westward-dipping limestone grades upsequence into an area of low-lying sandstone ridges. In the southwest corner of the map area, on the flanks of Cerro Bayo, sandstones and limestones of these two formations are again recognized, intermixed with voluminous rhyolites and occasional thin andesite flows. Locally, these rhyolites can be mapped as volcanic layers intercalated with the sedimentary rocks, but the largest areas of felsic rock appear to be flow domes, from which the volcanic horizons extend.

Cretaceous monzonite and gabbro intrusions

Cerro Bayo, located in the southwestern sector of the map, consists of Jurassic-Cretaceous-age volcano-sedimentary rocks intruded by quartz monzonite and hornblende gabbro bodies. The intrusive nature of these bodies is demonstrated by the presence of northeast-trending dikes that cut the volcano-sedimentary sequence and contact metamorphism adjacent to larger intrusions (calc-silicate hornfels alteration in calcareous sedimentary units and widespread epidotization). Furthermore, crosscutting relationships show that the hornblende gabbro postdates the quartz monzonite. A second such gabbro dike is found 7 km farther north (E485000 N7317000).

Two $^{40}Ar/^{39}Ar$ dates of 76.9 ± 1.2 and 74.0 ± 2.0 Ma have been obtained for hornblende from the Cerro Bayo gabbro (Table 3). These dates provide a Late Cretaceous minimum age for the Santa Ana Formation and the quartz monzonite intrusions, both of which the gabbro crosscuts.

The quartz monzonite intrusions are generally equigranular and medium grained, but some samples contain plagioclase phenocrysts (up to 3 mm long) and rare quartz phenocrysts, while quartz is abundant as an interstitial phase. The rocks are everywhere moderately altered, with chlorite replacing mafic phases, sericite replacing feldspars, and abundant scattered epidote. Alteration of feldspar phenocrysts makes estimation of modal plagioclase and alkali feldspar contents difficult, but preservation of granophyric textures (quartz-alkali feldspar intergrowths) suggests a monzonitic affinity. Calc-silicate alteration was observed where quartz monzonites intrude silty limestones near E488500 N7318000, with development of garnet and epidote in carbonate veins.

The hornblende gabbro ranges from porphyritic to ophitic in texture, with brown hornblende crystals locally exceeding 1 cm in length. Hornblende is intergrown with clinopyroxene (mostly chloritized) and plagioclase laths, with interstitial biotite and minor quartz. Propylitic alteration, in the form of chlorite, prehnite, secondary actinolite, and calcite, affects the groundmass.

Three samples of hornblende gabbro have been analyzed geochemically, and the results are listed in Table 4. The gabbro is the most mafic lithology sampled from the field area, averaging 45 wt percent SiO_2. It is also relatively rich in alkali elements ($Na_2O + K_2O$ = 3.3–5.0 wt %) and may be classified as a high K alkali gabbro (IUGS scheme, and alkalic-subalkalic division of Irvine and Baragar, 1971). Propylitic alteration may have affected alkali contents to some extent, but this is likely to have reduced their concentrations by, for example, chloritization of biotite, rather than enhanced them. Thus, the alkalic nature of these rocks seems to be primary in origin.

Additional support for an alkalic, as opposed to calc-alkalic, affinity for the gabbros is found in the trace element compositions, because normalized negative anomalies for Nb and Ti are not observed (Fig. 6A) and REE patterns show monotonic enrichments in the light elements (Fig. 6B). Mafic igneous rocks regionally related to subduction activity, but lacking the Nb-Ti-anomalies that are characteristic of arc magmas, are commonly found in back-arc settings where they may represent small-scale melting of the mantle in response to back-arc tectonic processes such as rifting (e.g., Fitton et al., 1988; Ringwood, 1990; Righter and Carmichael, 1992). Such an origin seems plausible for these intrusions, at a time when the main-arc activity was still farther west.

Paleocene-early Eocene (Augusta Victoria Formation)

Rapid convergence rates in the Paleocene and early Eocene epochs brought the focus of arc magmatism farther east into the Central Valley (Table 1). This activity was marked in the Escondida area by widespread andesitic and felsic volcanism, intercalated with arenaceous and calcareous sedimentation (the Augusta Victoria Formation). Like the Agua Dulce Formation, these volcanic sequences form regions of subdued, gravel-covered topography, with felsic volcanic horizons typically weathering to form low, poorly exposed ridges. The subcrop extent of this formation is thus poorly constrained, but it appears to underlie a significant proportion of the map area to the west of the Escondida-Zaldívar strands of the West Fissure zone. Structural disturbance has confused correlation of individual volcanic units in the area between Zaldívar and Chimborazo, but farther north, in an area of gentle open folding near E488000 N7340000, alternating sequences of andesitic lavas (locally vesicular) and felsic tuffs (displaying devitrification and eutaxitic textures) can be followed over an area of several square kilometers. These gently folded but subhorizontal volcanic sequences overlie the westward-dipping

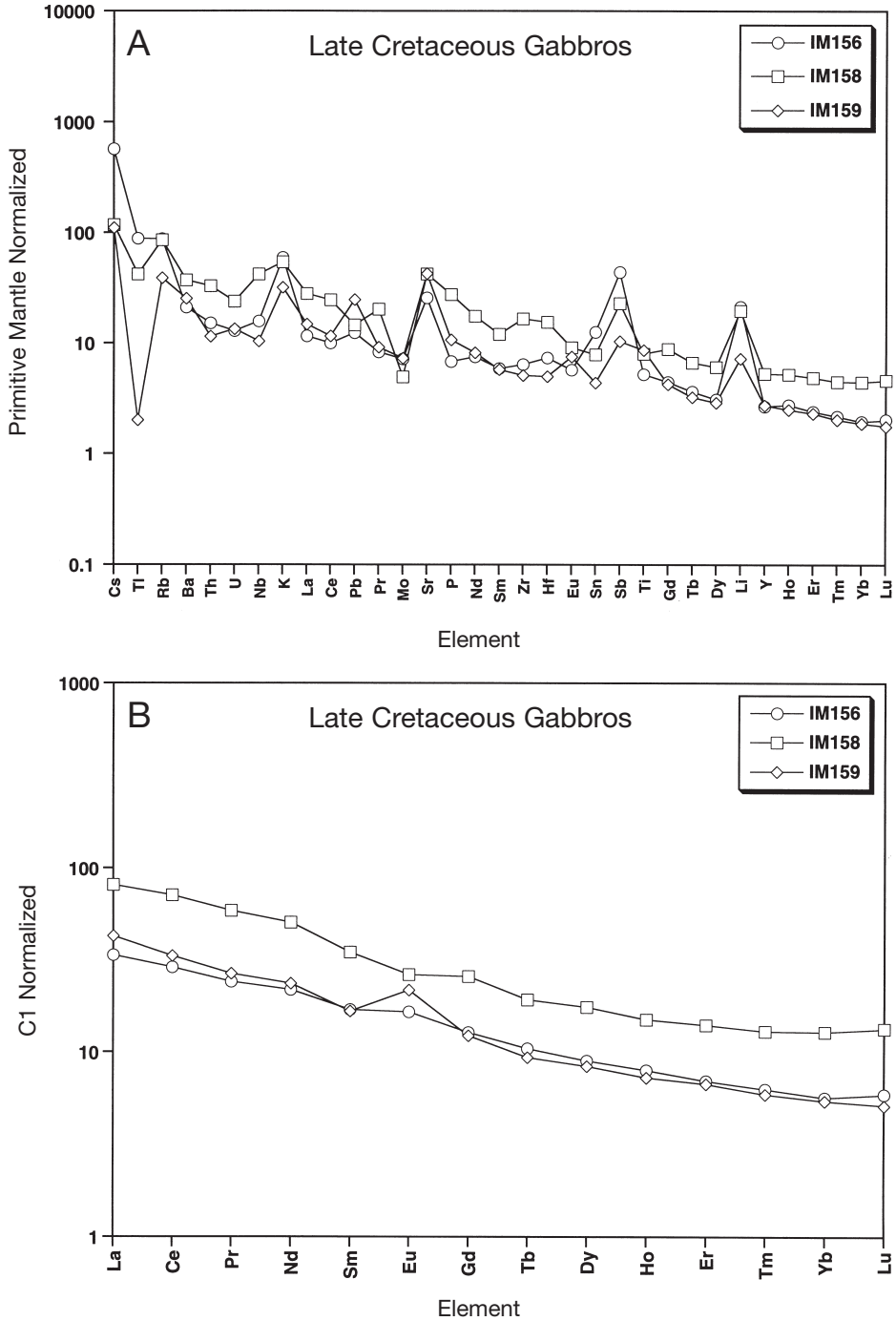

FIG. 6. Normalized trace element (A) and REE (B) diagrams for three samples of Cretaceous hornblende gabbro from Cerro Bayo. The gabbros display distinctive alkalic signatures (no Nb or Ti depletions), in contrast to the arc signatures of earlier and later igneous rocks from this area, and are believed to have been generated during a period of back-arc magmatic activity. Normalization values of Sun and McDonough (1989).

Mesozoic El Profeta and Santa Ana Formations with angular unconformity, most clearly observed near E488200 N7341500 and E490000 N7340000.

Marinovic et al. (1992) report a biotite K-Ar date of 55.0 ± 1.4 Ma for volcanic rocks from the base of the Augusta Victoria Formation near E486300 N7344200, a value consistent with other Paleocene-early Eocene dates for this formation from outside the map area. Petrographically and geochemically the andesitic lavas are unremarkable: they are mostly crystal rich, containing phenocrysts of plagioclase and clinopyroxene set in a fine-grained feldspathic matrix, and generally show some degree of propylitic (chlorite and epidote) alteration. The trace element and REE patterns for sample IM128 are similar to those of Triassic Agua Dulce Formation andesites but also to closely related late Eocene dioritic intrusions (Fig. 7; see below).

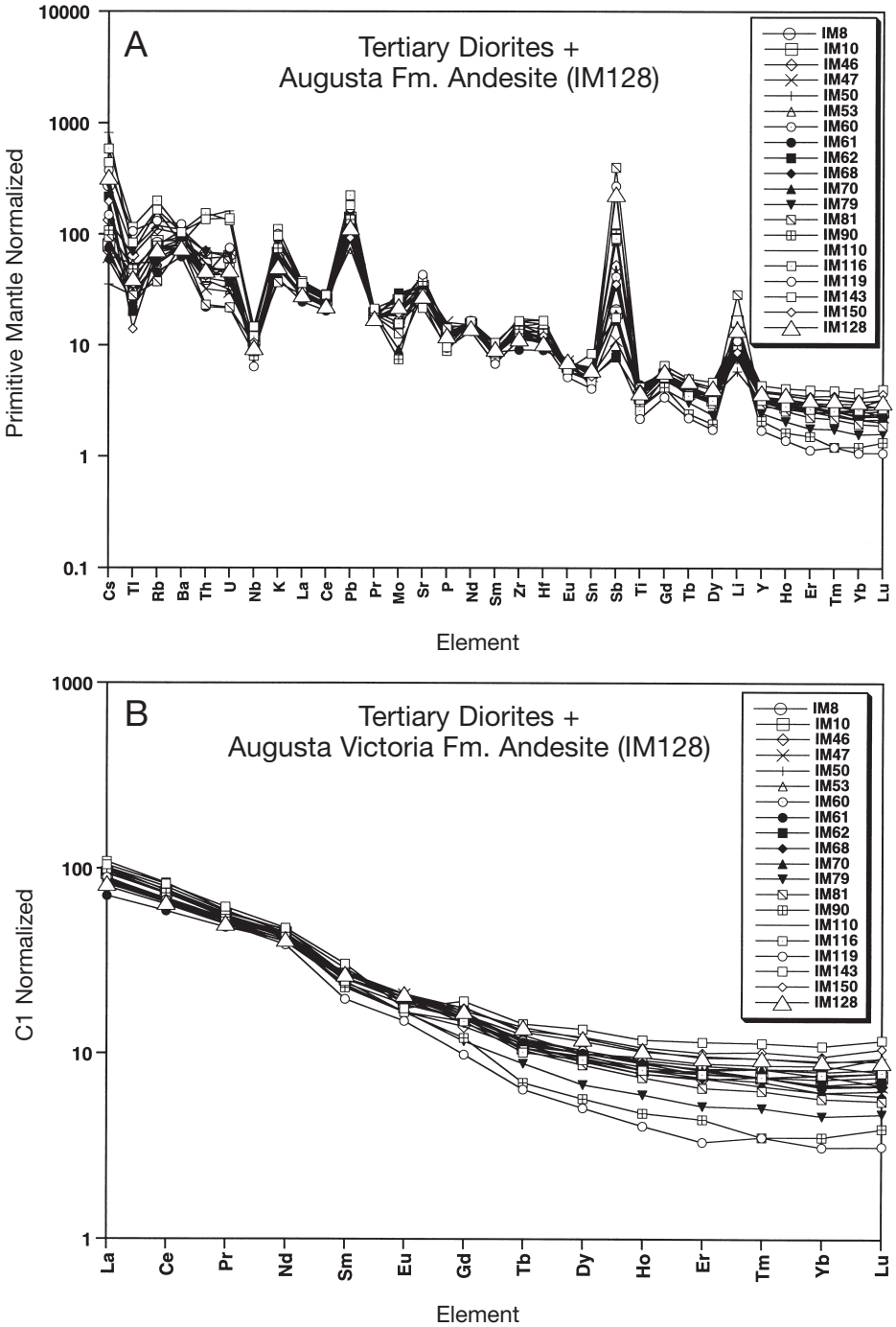

FIG. 7. Normalized trace element (A) and REE (B) diagrams for 19 samples of late Eocene-early Oligocene dioritic intrusive rocks and one sample of Paleocene-early Eocene (Augusta Victoria Formation) andesite. All of these rocks display closely similar, arclike trace element patterns, with smooth, listric-shaped REE profiles, suggesting control by hornblende fractionation. Normalization values of Sun and McDonough (1989).

Late Eocene-early Oligocene dioritic intrusions

Proprietary regional aeromagnetic maps reveal the presence of clusters of magnetic dioritic intrusions along the West Fissure zone, often spatially associated with mineralized porphyry centers. Such a cluster occurs around the Escondida-Zaldívar-Chimborazo porphyry group, extending westward beyond the present map limit but achieving greatest intensity in hills to the north, west, and east of Chimborazo. Dioritic stocks and dikes are most often found intruding rocks of the Augusta Victoria and El Profeta Formations. The diorites characteristically contain abundant hornblende phenocrysts and magnetite, indicating relatively high magmatic water contents and oxidation states (see below).

$^{40}Ar/^{39}Ar$ dating of hornblende has been carried out on six samples of these dioritic rocks from throughout the field area,

yielding dates between 38.28 ± 0.32 and 36.94 ± 0.46 Ma (Table 3). This age range is similar to that obtained for the emplacement of synmineralization porphyry intrusions at the Escondida, Zaldívar, and Chimborazo Cu deposits: 37.9 ± 1.1 Ma (Escondida porphyry); 38.7 ± 1.3 Ma (Llamo porphyry, Zaldívar); 38.09 ± 0.30 Ma (porphyry dike, Chimborazo). For example, sample IM79 (E501700 N7320200) was collected from a porphyritic andesite dike cutting a silica breccia body with hypogene advanced argillic alteration believed to be related to the Escondida hydrothermal system; the dike returned a date of 36.94 ± 0.46 Ma, marginally younger than the Escondida porphyry (37.9 ± 1.1 Ma; Richards et al., 1999).

Geochemically, the diorites compare closely to the composition of the Augusta Victoria Formation andesite as noted above: both lithologies are characterized by arclike trace element signatures (negative Ti and Nb anomalies), significant enrichments in Pb, Sb, and Li, and listric-shaped REE-enriched patterns lacking significant Eu anomalies (Fig. 7). In detail, these rocks show a trend of increasing heavy and middle REE depletion (light REE concentrations more or less static) with increasing differentiation, as measured by SiO_2 and MgO concentrations (Fig.8). Listric-shaped REE patterns during differentiation of intermediate-composition magmas are normally attributed to fractionation of middle + heavy REE-enriched hornblende (for which there is ample evidence in these hornblende-porphyritic diorites), whereas the absence of negative Eu anomalies may be due to high-magmatic oxidation states or suppression of feldspar fractionation (e.g., Frey et al., 1978; Hanson, 1980; Lopez, 1982; Lang and Titley, 1998). Such conditions arise where magmas contain sufficient water to stabilize hornblende as an early liquidus phase and suppress plagioclase crystallization. Burnham (1979) has estimated a minimum magmatic water content of 3 wt percent H_2O for the crystallization of amphibole in silicate melts, but higher water contents (>4 wt % H_2O) would be required for crystallization and segregation of hornblende as early, near-liquidus phenocrysts (e.g., Naney, 1983; Merzbacher and Eggler, 1984; Rutherford and Devine, 1988). Thus, the trace element data for these dioritic rocks indicate that they crystallized from relatively hydrous magmas, quite distinct from the drier, feldspar fractionation-controlled Paleozoic volcanic rocks (cf. Fig.4B).

Late Eocene-early Oligocene porphyry intrusions

As noted above, porphyritic intrusions associated with magmatic-hydrothermal Cu mineralization in the map area are coeval with the regional emplacement of hornblende diorite plutons. If the postmineralization Rhyolitic porphyry at Escondida is excluded (34.7 ± 1.7 Ma), dates for emplacement of synmineralization porphyry magmas at Escondida, Zaldívar, and Chimborazo overlap within error at ~38 Ma (Richards et al., 1999).

These three porphyries are andesitic to dacitic in composition (IUGS total alkali vs. silica classification scheme), with silica contents ranging from 60.5 wt percent (IM154: Chimborazo) to 67.7 wt percent (ZAL1: Llamo porphyry, Zaldívar). Their porphyritic textures and the degree of alteration (particularly of feldspars) make classification in terms of modal mineralogy difficult, but broadly speaking they are hypabyssal porphyritic equivalents of granodiorites. Mineralogically, the intrusions are characterized by abundant feldspar phenocrysts (plagioclase and less abundant alkali-feldspar), with subordinate quartz and biotite phenocrysts, set in a relatively fine grained quartzofeldspathic matrix. Hypogene alteration is ubiquitous, and some (but not all) of the biotite is secondary. Chloritization of this biotite is common, and sericitization of feldspars is extensively developed. In view of this alteration, little petrologic significance should be given to the alkali element concentrations of the samples listed in Table 4.

The reportedly postmineralization Rhyolitic porphyry at Escondida is, as its name suggests, rhyolitic in composition, and it is characterized by more abundant quartz phenocrysts than the synmineralization intrusions. Altered feldspar phenocrysts and relict biotite books are also present, set in a fine-grained matrix.

Trace element compositions of four samples of these porphyry intrusions are closely similar to those of the coeval diorites, differing only in accentuated depletions in Nb, P, Ti, and heavy REE, and enrichments in K, Pb, Mo, and Sb (doubtless in part due to hydrothermal introduction of the latter elements; Fig. 9A). Rare earth element patterns closely adhere to the general form of the diorite patterns but slope more steeply to lower middle and heavy REE values (Fig. 9B). Plots of La_n/Yb_n versus SiO_2 or MgO overlap and extend the range of data obtained from the diorites (Fig. 8), suggesting that the feldspar-biotite-quartz porphyries may be related to the diorites through fractionation. Hornblende has been replaced by biotite as a cotectic phase in these porphyries, however, reflecting decreasing CaO and/or a reduction in H_2O content in the melt with differentiation (Fig. 10; Naney, 1983; Rutherford and Hill, 1993; Candela, 1997). Because REE profiles for the diorites and porphyries mostly show no significant negative Eu anomalies (indeed, in many cases they show small positive anomalies; Fig. 11), feldspar fractionation does not seem likely to be the sole mechanism for the observed Ca depletion. Instead, the REE patterns are more consistent with hornblende fractionation, which will preferentially remove CaO as well as middle and heavy REE from the melt, and can generate small positive Eu anomalies. Once CaO concentrations in the melt fall below the level required for hornblende stability, biotite will replace this mineral as the supersolidus mafic phase:

$$5\ \text{K feldspar} + 2\ H_2O + 6\ Al_2O_{3(\text{melt})} + 3\ \text{tremolite} = 5\ \text{phlogopite} + 6\ \text{anorthite} + 12\ \text{quartz} \quad (1)$$

(in this equation, reactants may be components of mineral solid solutions or may be dissolved in the melt; Candela, 1997).

This mineralogical transition appears to have taken place at approximately 3 wt percent CaO and 65 wt percent SiO_2 in these magmas. Note, however, that subsolidus hydrothermal alteration may have modified the CaO concentrations of the porphyry samples to some degree, so these data should probably not be interpreted beyond this first-order observation.

In summary, the feldspar-biotite-quartz porphyries associated with mineralization at Escondida, Zaldívar, and Chimborazo are coeval and display geochemical affinities with a voluminous and regionally extensive suite of dioritic plutons. It is suggested that the porphyries were derived from this

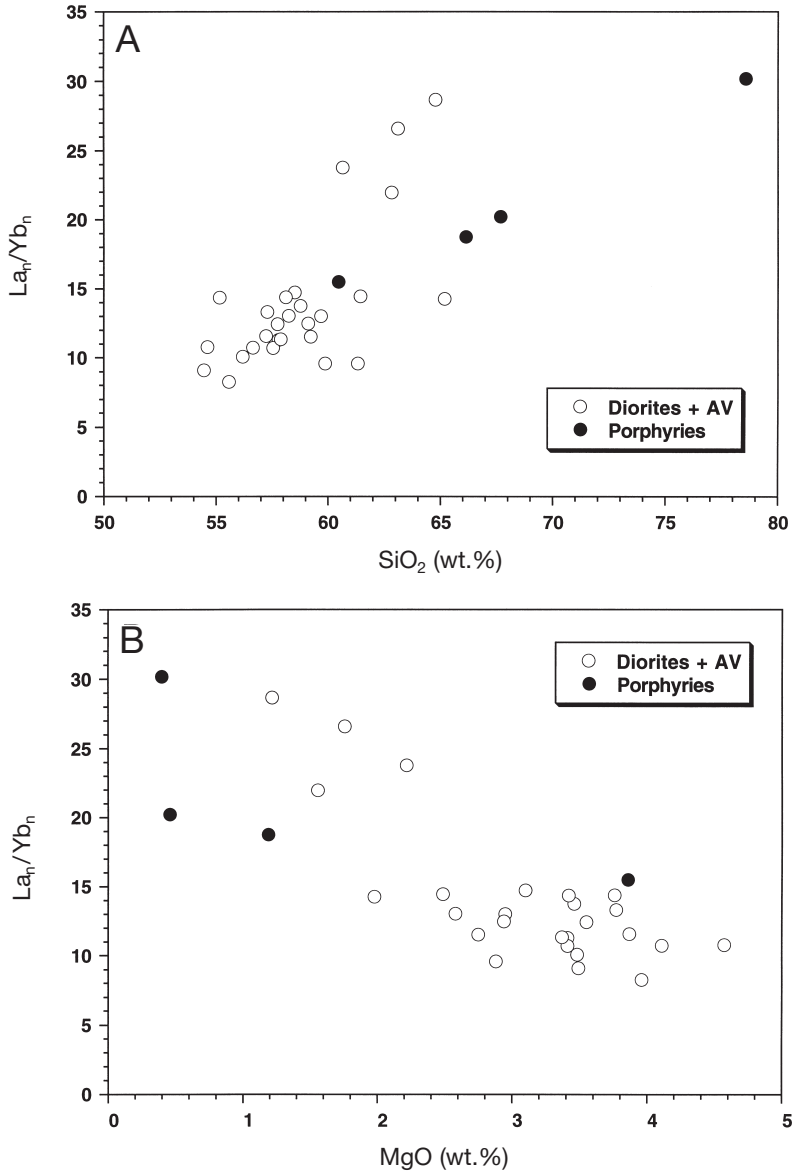

FIG. 8. Plots of C1-normalized La_n/Yb_n ratios (as a measure of light REE/heavy REE fractionation) vs. SiO_2 (A) and MgO (B) concentrations for Tertiary diorites, andesite (AV), and ore-related porphyry intrusions. A trend of increasing La_n/Yb_n ratio with differentiation from dioritic to rhyolitic compositions, combined with a lack of Eu depletion (Figs. 7B, 9B, 11), suggests that hornblende fractionation was important and indicates evolution of relatively hydrous, oxidized arc magmas. Normalization values of Sun and McDonough (1989).

dioritic magma largely by hornblende fractionation, and that they represent relatively evolved differentiates. The postmineralization Rhyolitic porphyry may represent a further, latest stage of magmatic differentiation to highly silicic compositions, but by this stage the magma appears to have lost the potential to generate significant Cu mineralization. Alternatively, its silicic composition may indicate a largely crustal origin, only indirectly related to the older dioritic magmatism.

U-Pb geochronology of these porphyries (Zentilli et al., 1994; Richards et al., 1999) has revealed the widespread presence of inherited zircons of Permo-Carboniferous age, similar to the age of the exposed intermediate to felsic volcanic basement in the area (La Tabla Formation). In addition to simple fractionation, therefore, it seems likely that these Tertiary magmas also assimilated crustal rocks. Isotopic studies are underway to investigate the extent and significance of such interactions, but the incorporation of crustal Pb and other components into porphyry magmas through assimilation processes is not an uncommon observation (e.g., Tilton et al., 1981; Sillitoe and Hart, 1984; Anthony and Titley, 1988; Hildreth and Moorbath, 1988; Williams, 1995).

Hydrothermal Activity in the Escondida District

An account of magmatic-hydrothermal and later epithermal-style mineralization in the Escondida porphyry Cu deposit is given by Padilla et al. (2001) and published information on

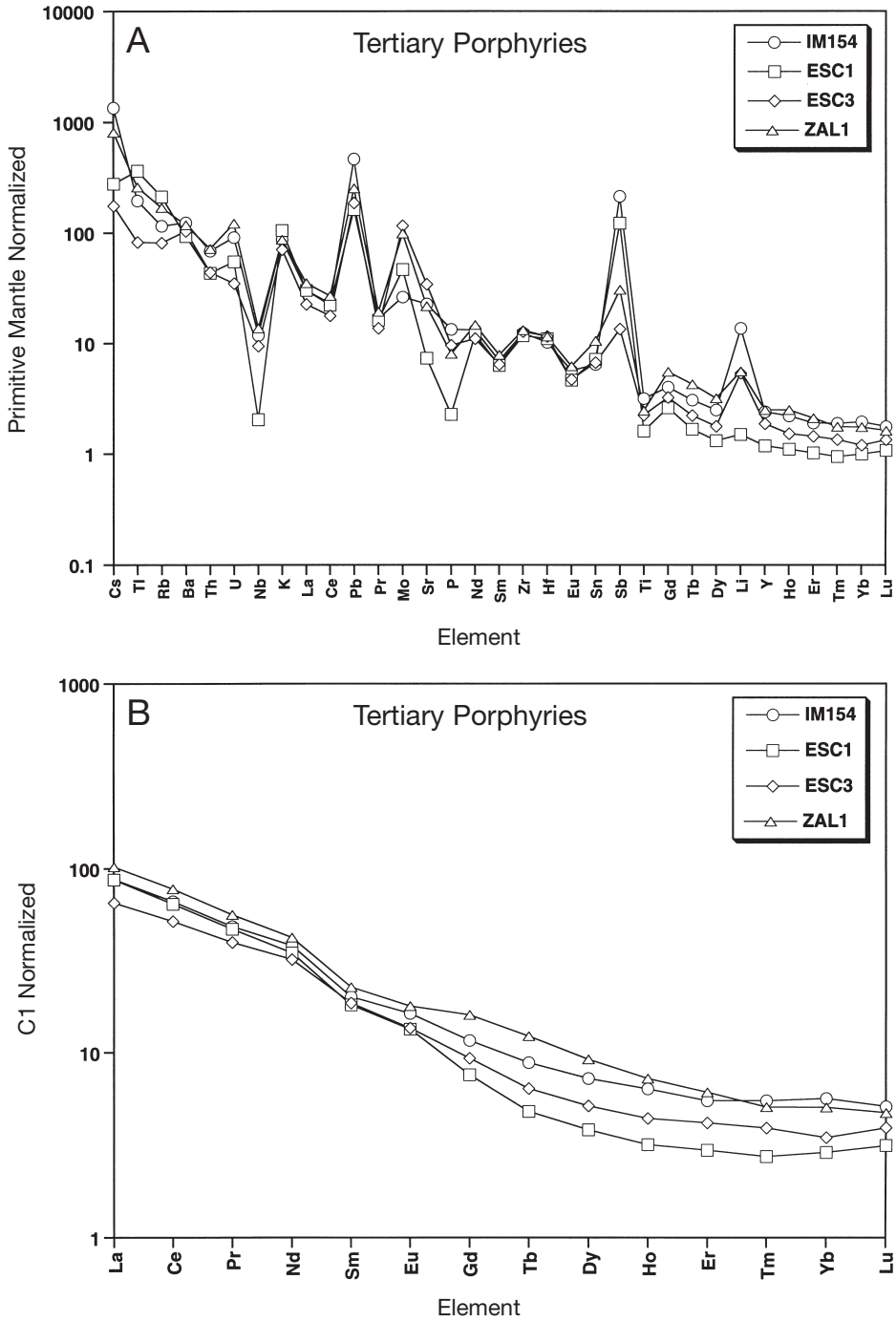

FIG. 9. Normalized trace element (A) and REE (B) diagrams for four samples of ore-related porphyry intrusions from Escondida, Zaldívar, and Chimborazo. Of these samples, the Chimborazo andesitic feldspar-biotite porphyry (IM154) is the most primitive (highest Pb, Sb, Li, and heavy REE), whereas the late mineralization Rhyolitic porphyry (ESC1) from Escondida is the most evolved (lowest Nb, P, Ti, and middle + heavy REE). None of these porphyries show significant Eu depletions (see also Fig. 11), indicating oxidizing conditions or suppression of plagioclase fractionation until late stages of magmatic differentiation. Normalization values of Sun and McDonough (1989).

the Zaldívar and Chimborazo deposits has been reviewed above. Hydrothermal alteration is not restricted to the limits of the deposits, however, but extends with variable intensity throughout the mapped region (Fig. 3). Some of this alteration may be unrelated to the Tertiary porphyry event, an example being the extensive silicification, phyllic alteration, and local tourmaline breccia formation observed in Paleozoic felsic volcanic rocks in the northeastern corner of the map area (near E498000 N7347000). No dates are currently available for this alteration, but other such areas of silicification in the basement rocks have been interpreted as being Paleozoic in age, and a tourmaline breccia Cu occurrence at La Casualidad

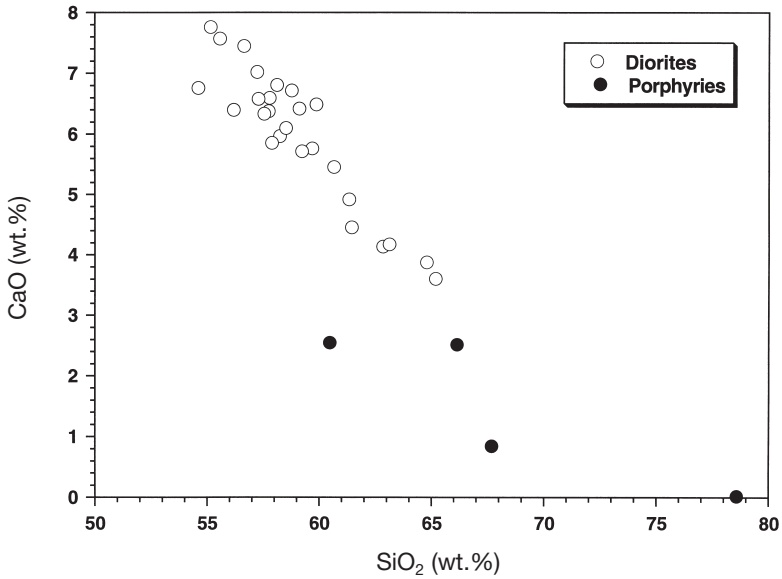

FIG. 10. A plot of CaO vs. SiO_2 concentration for Tertiary diorites and ore-related porphyry intrusions. The trend of decreasing CaO concentration with differentiation may explain the switch from hornblende to biotite predominance as a phenocryst phase in the evolved porphyries.

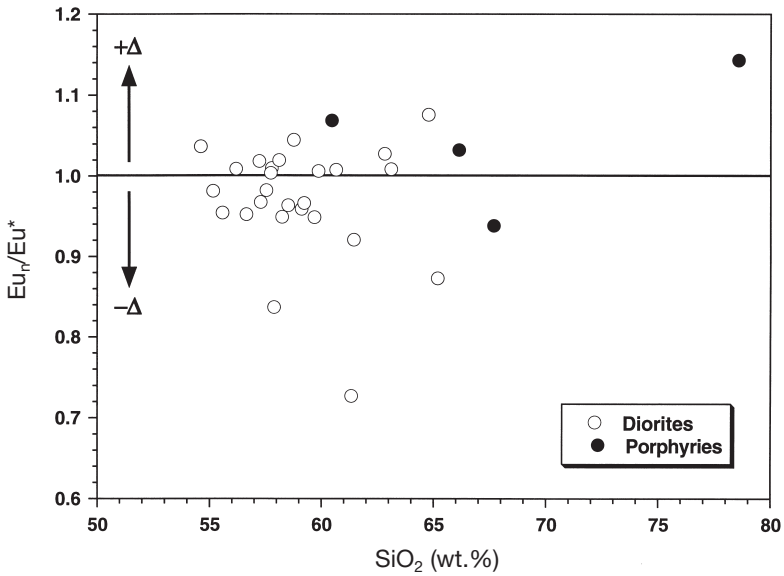

FIG. 11. A plot of Eu anomaly vs. SiO_2 for Tertiary diorites and ore-related porphyry intrusions. Zero or weakly positive Eu anomalies (+Δ) are consistent with oxidizing conditions and hornblende fractionation, whereas negative anomalies (–Δ) indicate plagioclase fractionation; the clustering of these data near $Eu_n/Eu^* = 1$ suggests that hornblende fractionation was dominant throughout the magmatic suite and is indicative of hydrous magmatic conditions. $Eu_n/Eu^* = Eu_n/\sqrt{Sm_n \times Gd_n}$; C1 normalization values of Sun and McDonough, 1989.)

(to the immediate southeast of the map area: E510600 N7313800) has been dated at 298 ± 7 Ma by Davidson et al. (1985).

In addition to this probable Paleozoic activity, localized calc-silicate alteration has been noted in the Cerro Bayo region, related to emplacement of Mesozoic plutons.

Regionally, the most widespread manifestations of hydrothermal activity are veins within the north-south and northwest structural corridors. Indeed, in the common absence of mappable outcrops of these structures, trails of quartz, jasper, carbonate, or barite float reliably indicate the locations and trends of individual faults. Barite veins, often over a meter in width and with occasional Cu colors, occur extensively along the northwest corridor in the east-central part of the map (e.g., E502000 N7329000), and also in the west, where numerous small pits and shafts have been dug by prospectors in the first half of the twentieth century (e.g., E485000 N7325000). Closer to the porphyry centers, however, these veins are

characterized by epithermal-style chalcedonic and vuggy quartz, increasing in intensity toward extensive zones of brecciation and silicification. Vapor-rich fluid inclusions are commonly observed in these quartz veins, indicating widespread boiling. Such alteration shows strongest development to the immediate north and east of Chimborazo and as a suite of silica breccia bodies with advanced argillic alteration to the east of Escondida and Zaldívar (the Baker breccias). A third zone of silicification and brecciation occurs along a strand of the West Fissure zone within andesites of the Augusta Victoria Formation near E493000 N7335000.

Alteration in the Baker breccias consists of pervasive silicification of fragmented volcanic country rocks, with coarse-grained hypogene alunite, granular diaspore, and kaolinite. Vapor phase and sparse high-salinity brine inclusions occur in quartz, consistent with models for advanced argillic alteration by condensation of acidic magmatic vapors (e.g., Brimhall and Ghiorso, 1983; Stoffregen, 1987; Hedenquist and Lowenstern, 1994). Although some Cu mineralization is associated with these breccias, drilling to date has not defined an economic resource. As noted above, a relatively unaltered andesitic porphyry dike cuts one of these breccia bodies, providing a minimum age for advanced argillic alteration of 36.94 ± 0.46 Ma (sample IM79).

The extent of this regional hydrothermal activity is much larger than the scale of, and is not focused on, individual stocks. This observation suggests that shallow-level plutonism and fluid flow were derived from and driven by deeper seated and more voluminous magmatism, consistent with evidence for fractionation of the porphyry magmas from a dioritic parent at depth, and contamination of these differentiated melts by assimilation of crustal rocks.

Structural Development of the Escondida District

The physical response of the north Chilean crust to deformation has been controlled largely by the compressive rigidity of the Paleozoic crystalline basement. Mesozoic back-arc extension broke up this crystalline slab along a series of arc-parallel normal faults, which became planes of weakness throughout subsequent deformation episodes (e.g., Günther et al., 1997). In addition to these arc-parallel structures, a series of long-lived northwest- and northeast-oriented cross-orogen lineaments may have influenced basement tectonics perhaps as far back as the late Precambrian (Salfity, 1985). Since the Mesozoic, therefore, the Paleozoic basement of northern Chile appears to have behaved as a disjointed set of rigid, fault-bounded blocks. Evidence for this behavior and its possible control on the localization of porphyry magmatism in the Escondida region is discussed below.

Mesozoic structures

Mesozoic transtensional strain led to the development of fault-bounded rift basins floored by downthrown Paleozoic blocks, which were filled by thick sequences of volcanic and sedimentary rocks, preserved in the field area as the Agua Dulce, El Profeta, and Santa Ana Formations (Mpodozis and Cornejo, 1997; Ardill et al., 1998). A transition to submarine conditions with deepening of the rift is interpreted to be indicated by the unconformable boundary between the Agua Dulce volcanic and El Profeta carbonate sequences, as described above.

A change to regional compression across the arc during the Cretaceous resulted in tilting, folding, and faulting of the Mesozoic sequence, followed by peneplanation prior to renewed deposition of Tertiary volcano-sedimentary sequences. Mesozoic exposures in the north of the map area are separated into two domains by an east-northeast–trending reverse fault. South of this fault, El Profeta and Santa Ana Formation sedimentary and intercalated volcanic rocks dip to the west at 20° to 80°, and little evidence of fault disruption is observed. To the north of the thrust fault, however, exposures of clastic sedimentary rocks of the Santa Ana Formation display numerous small-scale bedding-plane thrust faults (displacements of several meters only), with associated folding where faults step up through the sequence. This disruption results in complex, disjointed outcrop patterns. The northern block appears to be overthrust to the south, resulting in apparent duplication of the Santa Ana stratigraphy.

The strike and extent of the Mesozoic sequence in this northern area parallels the West fissure corridor, suggesting that an earlier manifestation of this structure may have controlled not only deposition but also compressional deformation of these rocks (cf. Günther et al., 1997).

In the southwestern corner of the field area, Mesozoic sedimentary and volcanic rocks again crop out, but here deformation patterns may have been modified by later intrusive events. A series of open folds with east-west axes are developed in El Profeta Formation rocks on the western flank of Cerro Bayo. These sequences appear to have been intruded and domed by monzonitic stocks and then block faulted along north-south- and west-northwest–trending structures. Late Cretaceous gabbro dikes and plugs were emplaced with northeast orientations, and crosscut the monzonites and structures developed within them, constraining this faulting event to the Late Cretaceous. The orientation and shape of the gabbro bodies suggest emplacement within tensional gashes, developed with long axes parallel to σ_1 (northeast) and inflating parallel to σ_3 (northwest). Such a stress field is consistent with renewed northeast-directed oblique subduction, initiated in the Late Cretaceous in response to a global increase in sea-floor spreading and convergence rates (Dalziel, 1986; Table 1).

Tertiary structures

Increased convergence rates at the start of the Tertiary brought the volcanic arc farther inland (Central Valley), with deposition of the Paleocene-early Eocene volcano-sedimentary Augusta Victoria Formation. In the Escondida area, these rocks are preserved within two basins: a northwest-trending fault-bounded trough between Chimborazo and Zaldívar, within which the volcano-sedimentary sequence is folded and disrupted along north-northwest–trending axes, and a less disturbed basin near E487000 N7340000. In this latter basin, mapping of a well-defined volcanic stratigraphy reveals open folding along north-northwest–trending gently plunging axes. These fold orientations are consistent with a northeast-directed principal stress direction.

Visible disruption along the northwest-trending Chimborazo-Zaldívar corridor postdates deposition of the Augusta Victoria

Formation. However, this corridor coincides with the regional northwest Archibarca lineament of Salfity (1985; Fig. 1), suggesting that it may be the supracrustal manifestation of a much larger, orogen-scale basement structure. Salfity (1985) shows sinistral displacement on these northwest-trending cross-orogen lineaments (see also Matteini et al., 1997; Abels and Bischoff, 1999), and the sense of drag shown in Augusta Victoria Formation outcrop patterns is consistent with this couple. Minor sinistral offsets are also recorded on northwest-trending faults mapped on the east side of the West Fissure zone (e.g., E497000 N7337000).

During this early Tertiary period, dextral strike-slip movement was initiated along the West Fissure zone (Maksaev and Zentilli, 1988; Reutter et al., 1991, 1996; Palacios et al., 1993; Lindsay et al., 1995). Dextral shear is consistent with shortening arising from oblique, northeast-directed convergence and would have caused compression or sinistral transpression along the northwest-trending structural corridor, as suggested by the folding observed in the Augusta Victoria Formation rocks (Fig. 12A).

In contrast to the Augusta Victoria Formation, the geometry of late Eocene intrusions does not appear to have been influenced by a compressive stress field. Instead, stocks are characterized by subcircular to bulbous shapes in map view (for example, in the area around E488000 N7334000, where diorite plugs pervasively intrude andesites of the Augusta Victoria Formation). Nevertheless, in a regional sense, the locus of emplacement of late Eocene plutons appears to be related to the intersection of the northwest corridor with the West Fissure zone. This relationship is perhaps most clearly shown by the porphyry centers themselves, all three of which are located either in the West Fissure zone (Escondida and Zaldívar) or the northwest corridor (Chimborazo) and within the zone of intersection of these structures.

As noted above, the stress field in the Cordillera de Domeyko appears to have changed around the time of porphyry emplacement in the late Eocene-early Oligocene, resulting in a switch from premineralization dextral to postmineralization sinistral movement in the West Fissure zone. Given that the plate convergence direction did not change significantly during this period, it is concluded that the regional stress field changed from σ_1 directed northeast to southeast (Fig. 12), thereby reversing the sense of movement in the West Fissure zone and related structures. Such a scenario would place the northwest corridor under tension in the late Eocene, with the potential to generate transtensional pull-apart basins at its intersection with the West Fissure zone (Fig. 12B). As was also noted above, such transtensional structures would be ideal loci for the shallow-level emplacement of magmas. The roughly rhombic shape of the Escondida intrusive system, for example, appears to fit this model well (cf. Ojeda, 1990).

Between 35 and 37 km of net, sinistral, postmineralization offset has been estimated along the West Fissure zone between Chuquicamata and El Abra (Dilles et al., 1997; Tomlinson and Blanco, 1997b). In the Escondida region, displacement may have been dispersed along several parallel strands of the West Fissure zone. Sinistral offsets are hard to confirm in this area because substantial vertical movements along the West fissure structures make correlations across the faults difficult. However, it is possible that the northwest-trending structural corridor observed in the east-central portion of the map area is the easterly continuation of the Archibarca lineament. In this case, a post-Eocene sinistral offset of between 20 and 25 km can be estimated across this part of the West Fissure zone.

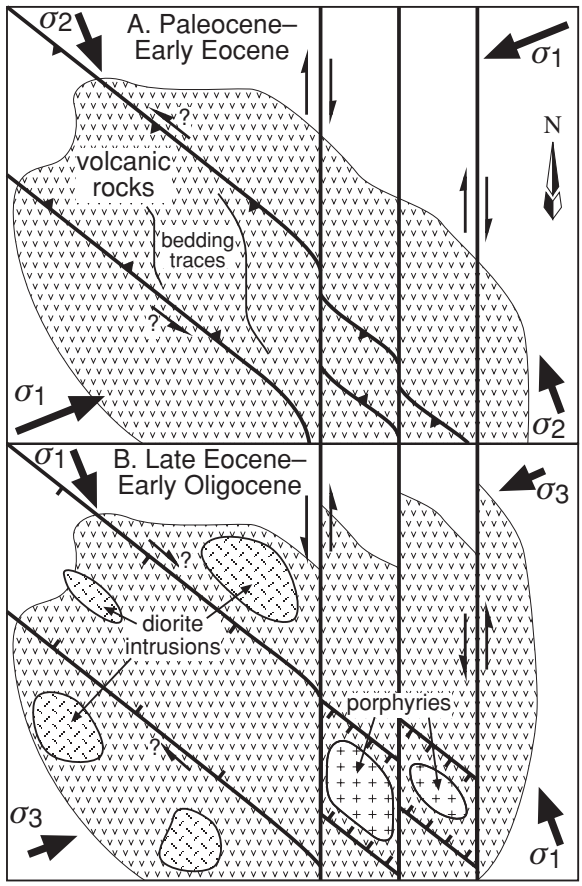

FIG. 12. Schematic model for structural development of the zone of intersection between the north-south West Fissure zone and the northwest-trending Archibarca lineament. A. Paleocene-early Eocene: Northeast-directed convergence caused compression or sinistral transpression along the northwest corridor and dextral transpression along the West Fissure zone, with the eruption of andesitic and rhyolitic flows and tuffs (Augusta Victoria Formation). B. Late Eocene-early Oligocene relaxation of convergent stresses reversed the sense of movement on the West Fissure zone and generated transtensional volumes within the zone of structural intersection. Dioritic magmas were emplaced within these dilational zones, fractionating and interacting with crustal rocks to generate evolved metalliferous porphyries. See text for discussion.

Model for Formation of Porphyry Cu Deposits in the Escondida District

The western seaboard of South America has been an active arc environment at least since the Mesozoic, with a volcanic history extending well into the Paleozoic. Porphyry Cu-forming magmatism has only occurred in very brief, spatially and temporally restricted pulses during this long history, however, with the largest deposits being formed in a single late Eocene-early Oligocene event.

Magmatism preceding this mid-Tertiary event is mostly of unremarkable, calc-alkaline composition and characterized by eruption of intermediate to felsic volcanic rocks. The only slightly unusual igneous rocks observed in the Escondida region are small alkali gabbro dikes and plugs related to Late Cretaceous back-arc processes, but the volume of these intrusions is small. Thus, there is no evidence for any unique characteristics or chemical preconditioning of the lithosphere that subsequently hosted the Escondida and related porphyry deposits (cf. Farmer and DePaolo, 1984; Dilles, 1987; Clark, 1995; Lang and Titley, 1998). Instead, the key processes that led to porphyry formation in this district are suggested to have been as follows:

1. A relatively prolonged and intense period of static arc magmatism (Paleocene-early Eocene Augusta Victoria Formation): The generation of primary arc magmas in the mantle wedge is not affected by processes in the upper plate. However, ascent of these magmas through the lithosphere will be controlled by upper-plate stress (Shaw, 1980; Hildreth, 1981). During periods of compression in the arc, magmas typically pool near the base of the lithosphere where they may undergo MASH-type interactions with lower crustal materials (MASH: melting, assimilation, storage, and homogenization; Hildreth and Moorbath, 1988). If the axis of arc magmatism remains static for an extended period of time, a considerable volume of modified magma will develop in the lower crust, with associated heating (Hildreth, 1981; Hutton, 1988; Pitcher, 1997; Clemens, 1998).

2. Changes in upper-plate stresses: Periodic stress relaxation, leading to localized extension or transtension are common features of arc tectonics (Hamilton, 1981, 1988; Weaver et al., 1987; Bott et al., 1989; Royden, 1993; Shemenda, 1993; Grocott et al., 1994; Pitcher, 1997). During such periods, modified and evolved magmas, accompanied by a major mantle-derived heat anomaly, are able to intrude in volume along dilational structures cutting the lithosphere (Hildreth, 1981; Hutton, 1988; Glazner, 1991; Petford and Atherton, 1992; Takada, 1994; Pitcher, 1997).

3. Upper-crustal ponding and fractionation: Ponding of these magmas in upper crustal magma chambers will lead to further crustal interaction and differentiation (AFC: assimilation and fractional crystallization; DePaolo, 1981). These hybrid magmas will evolve to increasingly felsic and volatile-rich compositions, which, when intruded as shallow-level stocks, may undergo devolatilization (Whitney, 1975; Burnham, 1979; Hildreth, 1981). Because these evolved stocks represent apophyses above a much larger volume of crystallizing magma, they act to focus the escape of volatiles and volatile-transported elements such as metals from a reservoir many times the volume of the host intrusion (Burnham, 1979; Burnham and Ohmoto, 1980; Dilles, 1987; Shinohara, 1994; Dilles and Proffett, 1995; Shinohara et al., 1995; Shinohara and Hedenquist, 1997).

Implications for localization of porphyry Cu deposits

The occurrence of several of the world's largest porphyry deposits within a single, narrow, coeval structural zone in the Chilean Andes has been recognized for many years (e.g., Sillitoe, 1981). It has also been proposed that the intersections of lithospheric-scale structures provide permeability for the voluminous ascent of arc magmas to shallow crustal levels (Rehrig and Heidrick, 1972; Seraphim and Hollister, 1976; Titley, 1981; Heidrick and Titley, 1982; Salfity, 1985; Sylvester and Linke, 1993; Sapiie and Cloos, 1995; Cornejo et al., 1997). During periods of compressive tectonism, such structures are largely closed and can only be penetrated by magmas under high pressure, resulting in dominance of effusive volcanism over shallow-level plutonism (Hildreth, 1981; Hutton, 1988; Glazner, 1991; Petford and Atherton, 1992; Takada, 1994; Pitcher, 1997). In contrast, during periods of differential stress relaxation, these structural intersections offer high-permeability pathways in three dimensions and can be intruded to shallow levels by dikes (along individual faults; Petford et al., 1994) or stocks (filling tension gashes or pull-apart volumes; Hutton, 1988; Glazner, 1991; Petford and Atherton, 1992; Paterson and Fowler, 1993; Pitcher, 1997). These structures may also localize the construction of composite volcanic edifices (Weaver et al., 1987; Takada, 1994), which have been suggested to overlie porphyry-forming systems (Sillitoe, 1973).

Dilles (1987), Cline and Bodnar (1991), and Cline (1995) have demonstrated from both field and theoretical observations that economic porphyry Cu deposits can be generated from a minimum volume of between 15 and 80 km^3 of normal calc-alkaline magma emplaced at pressures of between 0.5 and 2.0 kbars (depending on the compatibility behavior of Cu prior to water saturation). Although this volume of magma need not be exposed at the surface, it still implies that a significant-sized intrusion must underlie (at a relatively shallow level) any mineralized porphyry system. It is argued above that this requirement can best be fulfilled during periods of differential stress relaxation and in areas where the structural architecture can solve the space problem of igneous intrusion by providing dilational volumes. This theory is supported by observations from the Escondida region, which suggest that voluminous, shallow-level emplacement of dioritic to granodioritic magma in the late Eocene coincided with a switch from transpressive to transtensional tectonics in the West Fissure zone. Mapping has shown that the main center of porphyry magmatism and mineralization in this area lies within the area of intersection of the West Fissure zone and the Archibarca lineament, a regionally extensive northwest-trending structural corridor. This junction may have developed as a transtensional pull-apart volume, thereby offering a favorable locus for near-surface emplacement of magma.

Based on these observations and deductions, a general model is proposed in which porphyry Cu formation is optimized at times of stress relaxation in the arc and is localized by favorably oriented deep-seated structures. If this model is correct, then it is suggested that the following geologically observable features might be used as indicators for proximity (within ~10 km) to large porphyry centers:

1. Shallow-level dioritic plutonism within penecontemporaneous arc volcanic sequences: The switch from extrusive to intrusive magmatism may indicate relaxation of compressive stress in the arc, permitting the establishment of large upper crustal magma chambers. Exposure of plutonic rocks will be dependent on erosion level but this need not be great

because the depth of emplacement is believed to be very shallow (to the level of precursor volcanism in the Escondida area).

2. Voluminous, hydrous magmatism: Hornblende phenocrysts in plutonic phases indicate relatively high magmatic water contents (>4 wt % H_2O), necessary for the generation of magmatic-hydrothermal systems. Sufficient amounts of this magma are required to source the Cu in subsequent economic deposits.

3. Focal points for magmatic emplacement: Intersections of major, orogen-scale structures mark points of weakness and high permeability in the lithosphere. If these structures are favorably oriented under a low differential stress regime, transtensional pull-apart volumes may be formed into which magmas can readily pool at shallow crustal levels. The structures involved in such processes may have little surface expression, commonly being zones of basement heterogeneity or weakness inherited from earlier tectonic events and covered by younger volcanic and sedimentary sequences. Nevertheless, recognition on regional maps and Landsat images is often possible in the form of broad zones of supracrustal deformation, volcanicity, or facies changes in sedimentary basins. Such structural intersections may define targets of ~10-km-diameter or less.

All of the indicators proposed above can be identified quickly through regional geologic mapping and ground-truthed interpretation of satellite imagery and can provide a basis for the selection or rejection of first-pass exploration targets. The presence or absence of these indicators can be used to predict the potential or otherwise for emplacement of ore-forming magmas within a given area, but development of an ore deposit will additionally depend on local factors affecting that specific system.

It is suggested that these indicators are not restricted to porphyry localization in northern Chile but can be applied with appropriate regional modifications in any arc terrane, including oceanic island arcs.

Conclusions

Porphyry Cu-forming magmatism is shown to be coeval with regionally extensive late Eocene dioritic plutonism in the Escondida area and to be localized spatially by the intersection of two orogen-scale structural corridors. A comparison of the timing of porphyry emplacement to regional tectonic models suggests that plutonism occurred in response to stress relaxation following an extended period of early- to mid-Tertiary compression and volcanicity. Zones of intersection between orogen-parallel (north-south) and cross-orogen (northwest-southeast) translithospheric structures are suggested to have formed dilational conduits that facilitated the ascent and shallow-level emplacement of evolved arc magmas. The preceding period of arc compression may have resulted in pooling and evolution of these magmas near the base of the lithosphere, such that stress release permitted the sudden rise of large volumes of volatile and incompatible element-enriched magma, along with its contained heat.

Further fractionation of these hydrous, hornblende-porhyritic magmas in mid- to upper-crustal reservoirs led to the generation of dacitic biotite-porphyritic melts, which underwent volatile saturation upon emplacement as shallow-level apophyses. These apophyses may have provided conduits for fluids being exsolved from the larger body of crystallizing magma at depth and, therefore, became the foci for porphyry-type ore deposition.

On the basis of this analysis of porphyry formation in the Escondida region, several geologic features are suggested that can be recognized on a regional scale, which might indicate the potential for emplacement of large, potentially ore-forming magmatic systems. Principal among these criteria is the recognition of large (orogen-scale) structural corridors and, in particular, the intersections between such structures from regional mapping and interpretations of satellite imagery.

Voluminous, shallow-level emplacement (as opposed to extrusion) of arc magmas is thought to be promoted during periods of stress relaxation in the lithosphere. Evidence for a change to such conditions after a period of compression may be sought in a switch from widespread volcanism to shallow-level plutonism on a regional scale. Ore-forming plutonism may be restricted to a very narrow age range following this switch.

Development of potentially ore-forming magmatic-hydrothermal systems during crystallization of these magmas requires the release of large volumes of water through volatile saturation. Evidence for high initial water contents in the source magma may be provided by exposures of hornblende- or biotite-porphyritic hypabyssal intrusions. Clustering of such plutons may identify regions of intense magmatic activity, with the potential for extended fractionation and development of magmatic-hydrothermal systems.

Acknowledgments

This work was initiated with the support of grants from the Natural Environment Research Council (UK) and was completed with a grant from the Natural Sciences and Engineering Research Council (Canada). Fieldwork by JPR was supported by RTZ Mining and Exploration Ltd., and Minera Outokumpu Chile S.A., and special thanks are due to Mike Harris, Tim Beale, Gonzalo Mato, and Dave Andrews of RTZ (now Rio Tinto), and Tuomo Mäkelä, Carlos Llaumett, and Raul Venegas of Outokumpu. In addition, JPR thanks the several company *chofers* who accompanied him into the field at various times, and in particular Rudolfo Alvalos and Ivan Pastén. Manuel Durán of Minera Escondida Ltda., Tim Baker and Jorge Aceituno of Compañia Minera Zaldívar, Angelo Peri of Minera Cyprus Chile Ltda., and Christopher Hodgson of Minera Inmet Chile S.A. are thanked for access and permission to sample the deposits concerned. We thank Fin Stuart and Tony Fallick of the Scottish Universities Research and Reactor Centre for support and assistance with the argon analyses; Nick Marsh of the University of Leicester for XRF analyses; Brian Morgan of the University of Saskatchewan for ICP-MS analyses; and Philippe Erdmer and Robert Creaser of the University of Alberta for helpful scientific discussions.

The constructive reviews of John Dilles and two *Economic Geology* referees helped constrain our interpretations and improve the manuscript.

REFERENCES

Abels, A., and Bischoff, L., 1999, Clockwise block rotations in northern Chile: Indications for a large-scale domino mechanism during the middle-late Eocene: Geology, v. 27, p. 751–754.

Alpers, C.N., and Brimhall, G.H., 1988, Middle Miocene climatic change in the Atacama Desert, northern Chile: Evidence from supergene mineralization at La Escondida: Geological Society of America Bulletin, v. 100, p. 1640–1656.

——1989, Paleohydrologic evolution and geochemical dynamics of cumulative supergene metal enrichment at La Escondida, Atacama Desert, northern Chile: Economic Geology, v. 84, p. 229–255.

Andriessen, P.A.M., and Reutter, K.-J., 1994, K-Ar and fission track mineral age determinations of igneous rocks related to multiple magmatic arc systems along the 23° S latitude of Chile and northwest Argentina, *in* Reutter, K.J., Scheuber, E., and Wigger, P.J., eds., Tectonics of the southern central Andes; structure and evolution of an active continental margin: Berlin, Springer-Verlag, p. 141–153.

Anthony, E.Y., and Titley, S.R., 1988, Progressive mixing of isotopic reservoirs during magma genesis at the Sierrita porphyry copper deposit, Arizona: Inverse solutions: Geochimica et Cosmochimica Acta, v. 52, p. 2235–2249.

Ardill, J.R., Flint, S.S., Chong, G.D., and Wilke, H., 1998, Sequence stratigraphy of the Mesozoic Domeyko basin, northern Chile: Journal of the Geological Society of London, v. 155, p. 71–88.

Armijo, R., and Thiele, R., 1990, Active faulting in northern Chile: Ramp stacking and lateral decoupling along a subduction plate boundary?: Earth and Planetary Science Letters, v. 98, p. 40–61.

Bahlburg, H., and Hervé, F., 1997, Geodynamic evolution and tectonostratigraphic terranes of northwestern Argentina and northern Chile: Geological Society of America Bulletin, v. 109, p. 869–884.

Baker, R.C., and Guilbert, J.M., 1987, Regional structural control of porphyry copper deposits in northern Chile [abs.]: Geological Society of America Abstracts with Programs, v. 19, p. 578.

Boric, R., Díaz, F., and Maksaev, V., 1990, Geología y yacimientos metalíferos de la Región de Antofagasta: Servicio Nacional de Geología y Minería—Chile, Boletín, no. 40, 246 p.

Bott, M.P.H., Waghorn, G.D., and Whittaker, A., 1989, Plate boundary forces at subduction zones and trench-arc compression: Tectonophysics, v. 170, p. 1–15.

Brimhall, G.H, Jr., and Ghiorso, M.S., 1983, Origin and ore-forming consequences of the advanced argillic alteration process in hypogene environments by magmatic gas contamination of meteoric fluids: Economic Geology, v. 78, p. 73–90.

Brimhall, G.H, Jr., Alpers, C.N., and Cunningham, A.B., 1985, Analysis of supergene ore-forming processes and ground-water solute transport using mass balance principles: Economic Geology, v. 80, p. 1227–1256.

Brown, M., Diáz, F., and Grocott, J., 1993, Displacement history of the Atacama fault system 25°00' S–27°00' S, northern Chile: Geological Society of America Bulletin, v. 105, p. 1165–1174.

Burnham, C.W., 1979, Magmas and hydrothermal fluids, *in* Barnes, H.L., ed., Geochemistry of hydrothermal ore deposits, 2nd ed.: New York, J. Wiley Interscience, p. 71–136.

Burnham, C.W., and Ohmoto, H., 1980, Late-stage processes of felsic magmatism: Mining Geology Special Issue, no. 8, p. 1–11.

Bussell, M.A., 1976, Fracture control of high-level plutonic contacts in the Coastal Batholith of Peru: Proceedings of the Geologists Association, v. 87, p. 237–246.

Candela, P.A., 1997, A review of shallow, ore-related granites: Textures, volatiles, and ore metals: Journal of Petrology, v. 38, p. 1619–1633.

Chappell, B.W., and White, A.J.R., 1974, Two contrasting granite types: Pacific Geology, v. 8, p. 173–174.

Clark, A.H., 1995, Are outsize porphyry copper deposits either anatomically or environmentally distinctive? *in* Whiting, B.W., Mason, R., and Hodgson, C.J., eds., Giant ore deposits: Society of Economic Geologists Special Publication 2, p. 213–283.

Clark, A.H., Archibald, D.A., Lee, A.W., Farrar, E., and Hodgson, C.J., 1998, Laser probe $^{40}Ar/^{39}Ar$ ages of early- and late-stage alteration assemblages, Rosario porphyry copper-molybdenum deposit, Collahuasi district, I Region, Chile: Economic Geology, v. 93, p. 326–337.

Clemens, J.D., 1998, Observations on the origins and ascent mechanisms of granitic magmas: Journal of the Geological Society of London, v. 155, p. 843–851.

Cline, J.S., 1995, Genesis of porphyry copper deposits: The behavior of water, chloride, and copper in crystallizing melts: Arizona Geological Society Digest, v. 20, p. 69–82.

Cline, J.S., and Bodnar, R.J., 1991, Can economic porphyry copper mineralization be generated by a typical calc-alkaline melt?: Journal of Geophysical Research, v. 96, p. 8113–8126.

Coira, B., Davidson, J., Mpodozis, C., and Ramos, V., 1982, Tectonic and magmatic evolution of the Andes of northern Argentina and Chile: Earth-Science Reviews, v. 18, p. 303–332.

Cornejo, P., Tosdal, R.M., Mpodozis, C., Tomlinson, A.J., Rivera, O., and Fanning, C.M., 1997, El Salvador, Chile porphyry copper deposit revisited: Geologic and geochronologic framework: International Geology Review, v. 39, p. 22–54.

Dalziel, I.W.D., 1986, Collision and Cordilleran orogenesis: An Andean perspective: Geological Society of London Special Publication 19, p. 389–404.

Damm, K.-W., Pichowiak, S., Harmon, R.S., Todt, W., Kelley, S., Omarini, R., and Niemeyer, H., 1990, Pre-Mesozoic evolution of the central Andes; the basement revisited: Geological Society of America Special Paper 241, p. 101–126.

Damm, K.-W., Harmon, R.S., and Kelley, S., 1994, Some isotopic and geochemical constraints on the origin and evolution of the Central Andean basement (19°–24° S), *in* Reutter, K.J., Scheuber, E., and Wigger, P.J., eds., Tectonics of the southern central Andes; structure and evolution of an active continental margin: Berlin, Springer-Verlag, p. 263–276.

Davidson, J., Ramirez, C.F., Gardeweg, M., Herve, M., Brook, M., and Pankhurst, R., 1985, Late Palaeozoic-Early Triassic calderas and related mineralization in the Cordillera de Domeyko, northern Chile: Comunicaciones, no. 35, p. 53–57.

DePaolo, D.J., 1981, Trace element and isotopic effects of combined wall-rock assimilation and fractional crystallization: Earth and Planetary Science Letters, v. 53, p. 189–202.

de Silva, S.L., 1989, Altiplano-Puna volcanic complex of the central Andes: Geology, v. 17, p. 1102–1106.

Dilles, J.H., 1987, Petrology of the Yerington batholith, Nevada: Evidence for evolution of porphyry copper ore fluids: Economic Geology, v. 82, p. 1750–1789.

Dilles, J.H., and Proffett, J.M, 1995, Metallogenesis of the Yerington batholith, Nevada: Arizona Geological Society Digest, v. 20, p. 306–315.

Dilles, J.H., Tomlinson, A.J., Martin, M.W., and Blanco, N., 1997, El Abra and Fortuna complexes: A porphyry copper batholith sinistrally displaced by the Falla Oeste: Universidad Católica del Norte, VIII Congreso Geológico Chileno, Proceedings, p. 1883–1887.

Farmer, G.L., and DePaolo, D.J., 1984, Origin of Mesozoic and Tertiary granite in the western United States and implications for pre-Mesozoic crustal structure, 2. Nd and Sr isotopic studies of unmineralized and Cu- and Mo-mineralized granite in the Precambrian craton: Journal of Geophysical Research, v. 89, p. 10141–10160.

Fitton, J.G., James, D., Kempton, P.D., Ormerod, D.S., and Leeman, W.P., 1988, The role of lithospheric mantle in the generation of late Cenozoic basic magmas in the western United States: Journal of Petrology, Special Lithosphere Issue, p. 331–349.

Flint, S., Turner, P., Jolley, E.J., and Hartley, A.J., 1993, Extensional tectonics in convergent margin basins: An example from the Salar de Atacama, Chilean Andes: Geological Society of America Bulletin, v. 105, p. 603–617.

Franz, G., and Lucassen, F., 1997, Upper Paleozoic crustal thickening—the basement of the Sierra de Limon Verde in N-Chile (region Antofagasta): Universidad Católica del Norte, VIII Congreso Geológico Chileno, Proceedings, p. 1271–1274.

Frey, F.A., Chappell, B.W., and Roy, S.D., 1978, Fractionation of rare-earth elements in the Tuolumne Intrusive Series, Sierra Nevada batholith, California: Geology, v. 6, p. 239–242.

Frutos, J., 1981, Andean tectonics as a consequence of sea-floor spreading: Tectonophysics, v. 72, p. T21–T32.

——1988, Evolución de las trayectorias de esfuerzo en la tectónica de los Andes Meridionales: Congreso Geológico Chileno, V, Santiago, 8–12 August 1988, v. 1, p. A261–A281.

——1990, The Andes Cordillera: A synthesis of the geological evolution, *in* Fontboté, L., Amstutz, G.C., Cardozo, M., Cedillo, E., and Frutos, J., eds., Stratabound ore deposits in the Andes: Berlin, Springer-Verlag, p. 3–35.

Glazner, A.F., 1991, Plutonism, oblique subduction, and continental growth: An example from the Mesozoic of California: Geology, v. 19, p. 784–786.

Grocott, J., Brown, M., Dallmeyer, R.D., Taylor, G.K., and Treloar, P.J., 1994, Mechanisms of continental growth in extensional arcs: An example from the Andean plate-boundary zone: Geology, v. 22, p. 391–394.

Günther, A., Haschke, M., Reutter, K.-J., and Scheuber, E., 1997, Repeated reactivation of an ancient fault zone under changing kinematic conditions: the Sierra-de-Moreno fault system (SMFS) (N-Chilean Precordillera): Universidad Católica del Norte, VIII Congreso Geológico Chileno, Proceedings, p. 85–89.

Hamilton, W., 1981, Crustal evolution by arc magmatism: Royal Society of London Philosophical Transactions, ser. A, v. 301, p. 279–291.

——1988, Plate tectonics and island arcs: Geological Society of America Bulletin, v. 100, p. 1503–1527.

Hammerschmidt, K., Döbel, R., and Friedrichsen, H., 1992, Implications of $^{40}Ar/^{39}Ar$ dating of Early Tertiary volcanic rocks from the north-Chilean Precordillera: Tectonophysics, v. 202, p. 55–81.

Hanson, G.N., 1980, Rare earth elements in petrogenetic studies of igneous systems: Annual Review of Earth and Planetary Sciences, v. 8, p. 371–406.

Harmon, R.S., Barreiro, B.A., Moorbath, S., Hoefs, J., Francis, P.W., Thorpe, R.S., Déruelle, B., McHugh, J., and Viglino, J.A., 1984, Regional O-, Sr-, and Pb-isotope relationships in Cenozoic calc-alkaline lavas of the Andean Cordillera: Journal of the Geological Society of London, v. 141, p. 803–822.

Hedenquist, J.W., and Lowenstern, J.B., 1994, The role of magmas in the formation of hydrothermal ore deposits: Nature, v. 370, p. 519–527.

Heidrick, T.L., and Titley, S.R., 1982, Fracture and dike patterns in Laramide plutons and their structural and tectonic implications: American southwest, *in* Titley, S.R., ed., Advances in geology of the porphyry copper deposits: Tucson, University of Arizona Press, p. 73–91.

Heyl, A.V., 1972, The 38th Parallel lineament and its relationship to ore deposits: Economic Geology, v. 67, p. 879–894.

Hildreth, W., 1981, Gradients in silicic magma chambers: Implications for lithospheric magmatism: Journal of Geophysical Research, v. 86, p. 10,153–10,192.

Hildreth, W., and Moorbath, S., 1988, Crustal contributions to arc magmatism in the Andes of central Chile: Contributions to Mineralogy and Petrology, v. 98, p. 455–489.

Hutton, D.H.W., 1988, Granite emplacement mechanisms and tectonic controls: Inferences from deformation studies: Transactions of the Royal Society of Edinburgh, Earth Sciences, v. 79, p. 245–255.

Irvine, T.N., and Baragar, W.R.A., 1971, A guide to the chemical classification of the common volcanic rocks: Canadian Journal of Earth Sciences, v. 8, p. 523–548.

Jenner, G.A., Longerich, H.P., Jackson, S.E., and Fryer, B.J., 1990, ICP-MS—a powerful tool for high-precision trace element analysis in Earth sciences: Evidence from analysis of selected U.S.G.S. reference samples: Chemical Geology, v. 83, p. 133–148.

Jordan, T.E., and Gardeweg, M., 1989, Tectonic evolution of the late Cenozoic central Andes (20°–33°S): Oxford Monographs on Geology and Geophysics 8, p. 193–207.

Kay, S.M., Maksaev, V., Moscoso, R., Mpodozis, C., and Nasi, C., 1987, Probing the evolving Andean lithosphere: Mid–Late Tertiary magmatism in Chile (29°–30°30'S) over the modern zone of subhorizontal subduction: Journal of Geophysical Research, v. 92, p. 6173–6189.

Lahsen, A., 1982, Upper Cenozoic volcanism and tectonism in the Andes of northern Chile: Earth-Science Reviews, v. 18, p. 285–302.

Lang, J.R., and Titley, S.R., 1998, Isotopic and geochemical characteristics of Laramide magmatic systems in Arizona and implications for the genesis of porphyry copper deposits: Economic Geology, v. 93, p. 138–170.

Le Maitre, R.W., ed., 1989, A classification of igneous rocks and glossary of terms: Oxford, Blackwell Scientific Publications, 193 p.

Lindsay, D.D., Zentilli, M., and Rojas de la Rivera, J., 1995, Evolution of an active ductile to brittle shear system controlling mineralization at the Chuquicamata porphyry copper deposit, northern Chile: International Geology Review, v. 37, p. 945–958.

López, L., 1982, Características geoquímicas de rocas ígneas asociadas con pórfidos cupríferos chilenos: Revista Geológica de Chile, no. 17, p. 3–19.

López, V.M., 1939, The primary mineralization at Chuquicamata, Chile, S.A.: Economic Geology, v. 34, p. 674–711.

Lowell, J.D., 1991, The discovery of the La Escondida orebody: Economic Geology Monograph 8, p. 300–313.

Lowenstern, J.B., 1995, Applications of silicate-melt inclusions to the study of magmatic volatiles: Mineralogical Association of Canada Short Course, v. 23, p. 71–99.

Maksaev, V., and Zentilli, M., 1988, Marco metalogénico regional de los megadepósitos de tipo pórfido cuprífero del Norte Grande de Chile: Congreso Geológico Chileno, V, Santiago, 8–12 August 1988, v. 1, p. B181–B212.

Marinovic, N.S., Smoje, I.T., Maksaev, V.J., Herve, M.A., and Mpodozis, C.M., 1992, Carta geologica de Chile no. 70, Hoja Aguas Blancas: Santiago, Servicio Nacional de Geología y Mineria.

Matteini, M., Mazzuoli, R., and Omarini, R., 1997, The volcanism along the Calama-Olacapato-El Toro transversal fault system in the central Andes: The Tultul, del Dedio and Pocitos volcanoes (Puna, Argentina): Universidad Católica del Norte, VIII Congreso Geológico Chileno, Proceedings, p. 159–163.

McKee, E.H., and Noble, D.C., 1989, Cenozoic tectonic events, magmatic pulses, and base- and precious-metal mineralization in the central Andes: Circum-Pacific Council for Energy and Mineral Resources Earth Science Series, v. 11, p. 189–194.

McNulty, B.A., Farber, D.L., Wallace, G.S., Lopez, R., and Palacios, O., 1998, Role of plate kinematics and plate-slip-vector partitioning in continental magmatic arcs: Evidence from the Cordillera Blanca, Peru: Geology, v. 26, p. 827–830.

Merzbacher, C., and Eggler, D.H., 1984, A magmatic geohygrometer: Application to Mount St. Helens and other dacitic magmas: Geology, v. 12, p. 587–590.

Mining Annual Review, 1997: London, Mining Journal Ltd., 240 p.

Mining Journal, 1999: London, Mining Journal Ltd., v. 332, p. 477.

Mortimer, C., 1973, The Cenozoic history of the southern Atacama Desert, Chile: Journal of the Geological Society of London, v. 129, p. 505–526.

——1980, Drainage evolution in the Atacama Desert of northern Chile: Revista Geológica de Chile, no. 11, p. 3–28.

Mpodozis, C., and Allmendinger, W., 1993, Extensional tectonics, Cretaceous Andes, northern Chile (27°S): Geological Society of America Bulletin, v. 105, p. 1462–1477.

Mpodozis, C., and Cornejo, P., 1997, El rift Triásico-Sinemuriano de Sierra Exploradora, Cordillera de Domeyko (25°–26°S): Asociaciones de facies y reconstrucción tectonica: Universidad Católica del Norte, VIII Congreso Geológico Chileno, Proceedings, p. 550–554.

Mpodozis, C., and Ramos, V., 1989, The Andes of Chile and Argentina: Circum-Pacific Council for Energy and Mineral Resources Earth Science Series, v. 11, p. 59–90.

Naney, M.T., 1983, Phase equilibria of rock-forming ferromagnesian silicates in granitic systems: American Journal of Science, v. 283, p. 993–1033.

Ojeda, J.M., 1986, Escondida porphyry copper deposit, II Region, Chile: Exploration drilling and current geological interpretation, *in* Mining Latin America: Papers presented at the Mining Latin America conference, Santiago, 17–19 November 1986: London, Institute of Mining and Metallurgy, p. 299–318.

——1990, Geology of the Escondida porphyry copper deposit, II Region, Chile, *in* Pacific Rim 90 Congress, Gold Coast, Queensland: Australasian Institute of Mining and Metallurgy, p. 473–483.

Padilla, H., 1988, Eventos intrusivos y deformaciónes en la Cordillera de Domeyko a la latitud del salar de Punta Negra. Antecedentes geocronológicos K-Ar: Congreso Geológico Chileno, V, Santiago, 8–12 August 1988, v. 3, p. I229–I243.

Padilla-Garza, R.A., Titley, S.R., and Pimentel B., F., 2001, Geology of the Escondida porphyry copper deposit, Antofagasta region, Chile: Economic Geology, v. 96, p. 307–324.

Palacios, C.M., Townley, B.C., Lahsen, A.A., and Egaña, A.M., 1993, Geological development and mineralization in the Atacama segment of the South American Andes, northern Chile (26°15'–27°25'S): Geologische Rundschau, v. 82, p. 652–662.

Pardo-Casas, F., and Molnar, P., 1987, Relative motion of the Nazca (Farallon) and South American plates since Late Cretaceous time: Tectonics, v. 6, p. 233–248.

Paterson, S.R., and Fowler, T.K., 1993, Extensional pluton-emplacement models: Do they work for large plutonic complexes? Geology, v. 21, p. 781–784.

Petersen, C.R., Rivera, S.L., and Peri, M.A., 1994, Chimborazo copper deposit, II Region, Chile: Geology and exploration [abs.]: 7° Congreso Geológico Chileno, Actas Volumen II, p. 1613.

——1996, Chimborazo copper deposit, Region II, Chile: Exploration and geology: Society of Economic Geologists Special Publication 5, p. 71–80.

Petford, N., and Atherton, M.P., 1992, Granitoid emplacement and deformation along a major crustal lineament: The Cordillera Blanca, Peru: Tectonophysics, v. 205, p. 171–185.

Petford, N., Lister, J.R., and Kerr, R.C., 1994, The ascent of felsic magmas in dykes: Lithos, v. 32, p. 161–168.

Pichler, H., and Zeil, W., 1972, The Cenozoic rhyolite-andesite association of the Chilean Andes: Bulletin Volcanologique, v. 35, p. 424–452.

Pilger, R.H., 1983, Kinematics of the South American subduction zone from global plate reconstructions: American Geophysical Union Geodynamics Series, v. 9, p. 113–125.

Pitcher, W.S., 1997, The nature and origin of granite, 2nd ed.: London, Chapman and Hall, 387 p.

Rehrig, W.A., and Heidrick, T.L., 1972, Regional fracturing in Laramide stocks of Arizona and its relationship to porphyry copper mineralization: Economic Geology, v. 67, p. 198–213.

Reutter, K.-J., and Scheuber, E., 1988, Relation between tectonics and magmatism in the Andes of northern Chile and adjacent areas between 21° and 25° S: Congreso Geológico Chileno, V, Santiago, 8–12 August 1988, v. 1, p. A345–A363.

Reutter, K.-J., Scheuber, E., and Helmcke, D., 1991, Structural evidence of orogen-parallel strike slip displacements in the Precordillera of northern Chile: Geologische Rundschau, v. 80, p. 135–153.

Reutter, K.-J., Scheuber, E., and Chong, G., 1996, The Precordilleran fault system of Chuquicamata, northern Chile: Evidence for reversals along arc-parallel strike-slip faults: Tectonophysics, v. 259, p. 213–228.

Richards, J.P., Noble, S.R., and Pringle, M.S., 1999, A revised late Eocene age for porphyry Cu magmatism in the Escondida area, northern Chile: Economic Geology, v. 94, p. 1231–1247.

Righter, K., and Carmichael, I.S.E., 1992, Hawaiites and related lavas in the Atenguillo graben, western Mexican volcanic belt: Geological Society of America Bulletin, v. 104, p. 1592–1607.

Ringwood, A.E., 1990, Slab-mantle interactions. 3. Petrogenesis of intraplate magmas and structure of the upper mantle: Chemical Geology, v. 82, p. 187–207.

Royden, L.H., 1993, The tectonic expression slab pull at continental convergent boundaries: Tectonics, v. 12, p. 303–325.

Rutherford, M.J., and Devine, J.D., 1988, The May 18, 1980, eruption of Mount St. Helens. 3. Stability and chemistry of amphibole in the magma chamber: Journal of Geophysical Research, v. 93, p. 11,949–11,959.

Rutherford, M.J., and Hill, P.M., 1993, Magma ascent rates from amphibole breakdown: An experimental study applied to the 1980–1986 Mount St. Helens eruptions: Journal of Geophysical Research, v. 98, p. 19,667–19,685.

Salfity, J.A., 1985, Lineamientos transversales al rumbo andino en el noroeste Argentino: Congreso Geológico Chileno, IV, Antofagasta, August 1985, Part 2, p. 119–137.

Salfity, J.A., and Gorustovich, S.A., 1998, The geological evolution of the province of Salta (Argentina) and neighboring regions: Ministry of Production and Employment, Secretariat of Mining, Industry and Energy Resources, Salta, Argentina, Atlas of 67 figures with explanations.

Sapiie, B., and Cloos, M., 1995, Strike-slip faulting and related veining in the Grasberg porphyry Cu-Au ore system, Gunung Bijih (Ertsberg) mining district, Irian Jaya, Indonesia (West New Guinea) [abs.]: Geological Society of America Abstracts with Programs, v. 27, p. A–377.

Scheuber, E., and Andriessen, P.A.M., 1990, The kinematic and geodynamic significance of the Atacama fault zone, northern Chile: Journal of Structural Geology, v. 12, p. 243–257.

Scheuber, E., and Reutter, K.-J., 1992, Magmatic arc tectonics in the Central Andes between 21° and 25°S: Tectonophysics, v. 205, p. 127–140.

Scheuber, E., Bogdanic, T., Jensen, A., and Reutter, K.-J., 1994, Tectonic development of the north Chilean Andes in relation to plate convergence and magmatism since the Jurassic, *in* Reutter, K.J., Scheuber, E., and Wigger, P.J., eds., Tectonics of the southern Central Andes: Structure and evolution of an active continental margin: Berlin, Springer-Verlag, p. 121–139.

Seraphim, R.H., and Hollister, V.F., 1976, Structural settings: Canadian Institute of Mining and Metallurgy Special Volume 15, p. 30–43.

Shaw, H.R., 1980, The fracture mechanisms of magma transport from the mantle to the surface, *in* Hargraves, R.B., ed., Physics of magmatic processes: Princeton, NJ, Princeton University Press, p. 201–264.

Shemenda, A.I., 1993, Subduction of the lithosphere and back arc dynamics: Insights from physical modeling: Journal of Geophysical Research, v. 98, p. 16,167–16,185.

Shinohara, H, 1994, Exsolution of immiscible vapor and liquid phases from a crystallizing silicate melt: Implications for chlorine and metal transport: Geochimica et Cosmochimca Acta, v. 58, p. 5215–5221.

Shinohara, H., and Hedenquist, J.W., 1997, Constraints on magma degassing beneath the Far Southeast porphyry Cu-Au deposit, Philippines: Journal of Petrology, v. 38, p. 1741–1752.

Shinohara, H, Kazahaya, K., and Lowenstern, J.B., 1995, Volatile transport in a convecting magma column: Implications for porphyry Mo mineralization: Geology, v. 23, p. 1091–1094.

Sillitoe, R.H., 1973, The tops and bottoms of porphyry copper deposits: Economic Geology, v. 68, p. 799-815.

——1981, Regional aspects of the Andean porphyry copper belt in Chile and Argentina: Transactions of the Institute of Mining and Metallurgy, v. 90, p. B15–B36.

——1992, Gold and copper metallogeny of the central Andes: Past, present, and future exploration objectives: Economic Geology, v. 87, p. 2205–2216.

Sillitoe, R.H., and Hart, S.R., 1984, Lead-isotope signatures of porphyry copper deposits in oceanic and continental settings, Colombian Andes: Geochimica et Cosmochimica Acta, v. 48, p. 2135–2142.

Sillitoe, R.H., and McKee, E.H., 1996, Age of supergene oxidation and enrichment in the Chilean porphyry copper province: Economic Geology, v. 91, p. 164–179.

Singer, B.S., and Pringle, M.S., 1996, The age and duration of the Matuyama-Bruhnes geomagnetic polarity reversal from $^{40}Ar/^{39}Ar$ incremental heating analyses of lavas: Earth and Planetary Science Letters, v. 139, p. 47–61.

Smoje, I., and Marinovic, N., 1994, Intrusivos del Carbonifero Permico en la Cordillera de Domeyko: Nuevos antecedentes radiometricos: Universidad de Concepcion, 7° Congreso Geológico Chileno, Proceedings, p. 1213–1216.

Stoffregen, R., 1987, Genesis of acid-sulfate alteration and Au-Cu-Ag mineralization at Summitville, Colorado: Economic Geology, v. 82, p. 1575–1591.

Sun, S.-S., and McDonough, W.F., 1989, Chemical and isotopic systematics of oceanic basalts: Implications for mantle composition and processes: Geological Society of London Special Publication 42, p. 313–345.

Sylvester, H., and Linke, M., 1993, Structural control of intrusions and hydrothermal alteration zones by intersecting fault systems in the Cretaceous magmatic arc of the southern Central Andes at 27°S, III. Region, Chile: Zentralblattes für Geologie und Paläontologie, v. 1, p. 361–376.

Takada, A., 1994, The influence of regional stress and magmatic input on styles of monogenetic and polygenetic volcanism: Journal of Geophysical Research, v. 99, p. 13,563–13,573.

Tilton, G.R., Pollak, R.J., Clark, A.H., and Robertson, R.C.R., 1981, Isotopic composition of Pb in central Andean ore deposits: Geological Society of America Memoir 154, p. 791–816.

Titley, S.R., 1981, Geologic and geotectonic setting of porphyry copper deposits in the southern Cordillera: Arizona Geological Society Digest, v. 14, p. 79–97.

Tobisch, O.T., and Cruden, A.R., 1995, Fracture-controlled magma conduits in an obliquely convergent continental magmatic arc: Geology, v. 23, p. 941–944.

Tomlinson, A.J., and Blanco, N., 1997a, Structural evolution and displacement history of the West fault system, Precordillera, Chile: Pt 1. Synmineral history: Universidad Católica del Norte, VIII Congreso Geológico Chileno, Proceedings, p. 1873–1877.

——1997b, Structural evolution and displacement history of the West fault system, Precordillera, Chile: Pt. 2. Postmineral history: Universidad Católica del Norte, VIII Congreso Geológico Chileno, Proceedings, p. 1878–1882.

Weaver, C.S., Grant, W.C., and Shemeta, J.E., 1987, Local crustal extension at Mount St. Helens, Washington: Journal of Geophysical Research, v. 92, p. 10,170–10,178.

Whitney, J.A., 1975, Vapor generation on a quartz monzonite magma: A synthetic model with application to porphyry copper deposits: Economic Geology, v. 70, p. 346–358.

Williams, W.C., 1995, The crustal heritage of ore deposits in northern Chile [abs.]: Geological Society of America Abstracts with Programs, v. 27, p. A–410.

Woodward, L.A., 1984, Basement control of Tertiary intrusions and associated mineral deposits along Tijeras-Cañoncito fault system, New Mexico: Geology, v. 12, p. 531–533.

Yáñez, G., Mpodozis, C., and Tomlinson, A.J., 1994, Eocene dextral oblique convergence and sinistral shear along the Domeyko fault system: A thin viscous sheet approach with asthenospheric drag at the base of the crust: Universidad de Concepcion, 7° Congreso Geológico Chileno, Proceedings, p. 1478–1482.

Zentilli, M., Krogh, T.E., Maksaev, V., and Alpers, C.N., 1994, Uranium-lead dating of zircons from the Chuquicamata and La Escondida porphyry copper deposits, Chile: Inherited zircon cores of Paleozoic age with Tertiary overgrowths: Comunicaciones, no. 45, p. 101–110.